Copyright Warning & Restrictions

The copyright law of the United States (Title 17, United States Code) governs the making of photocopies or other reproductions of copyrighted material.

Under certain conditions specified in the law, libraries and archives are authorized to furnish a photocopy or other reproduction. One of these specified conditions is that the photocopy or reproduction is not to be "used for any purpose other than private study, scholarship, or research." If a, user makes a request for, or later uses, a photocopy or reproduction for purposes in excess of "fair use" that user may be liable for copyright infringement,

This institution reserves the right to refuse to accept a copying order if, in its judgment, fulfillment of the order would involve violation of copyright law.

Please Note: The author retains the copyright while the New Jersey Institute of Technology reserves the right to distribute this thesis or dissertation

Printing note: If you do not wish to print this page, then select "Pages from: first page # to: last page #" on the print dialog screen

ABSTRACT

CARBON FIBER ELECTRODES FOR *IN VIVO* NEURAL RECORDING

by
Esma Cetinkaya

Multi-channel micro electrodes for neural recording is a growing field that thrives on novel materials and fabrication techniques offered by micro fabrication technology. The material and the design of microelectrodes have a critical role on the quality of neural signals recorded. The neural signals collected by chronic implantation of these devices in experimental animals reveal new information about the brain functions and guide the development of new diagnostic and treatment options for neurological disorders.

Ideally, a microelectrode should meet two important criteria: longevity after implantation and minimal tissue insult. Carbon fibers` high tensile strength and flexibility allow fabrication of micro-scale electrodes that can withstand mechanical challenges in mobile parts of the CNS. Although there are studies showing carbon fibers' superior qualities as a potential electrode material, these studies are mostly restricted to the brain cortex. There is a need for microelectrode designs that can survive long implantation times in the moving parts of the CNS like the spinal cord.

In this study, carbon fiber microelectrode (CFME) bundles were developed and tested in the spinal cord of experimental animals for neural recording. Neural data analysis revealed that desheathing the tips of the fibers decreased spike counts, but increased signal-to-noise ratios. Triple carbon fibers in parallel did not improve the signal quality as much as desheathing. Lastly, immunohistochemistry showed that electrode tips were splayed in tissue after implantation and each had a small footprint with mild

encapsulation around. These results are very promising for the use of carbon fiber bundle electrodes for chronic neural recording in survival studies.

CARBON FIBER ELECTRODES FOR *IN VIVO* NEURAL RECORDING

by
Esma Cetinkaya

A Thesis
Submitted to the Faculty of
New Jersey Institute of Technology
in Partial Fulfillment of the Requirements for the Degree of
Master of Science in Biomedical Engineering

Department of Biomedical Engineering

December 2017

APPROVAL PAGE

CARBON FIBER ELECTRODES FOR *IN VIVO* NEURAL RECORDING

Esma Cetinkaya

Dr. Mesut Sahin, Thesis Advisor — Date
Professor of Biomedical Engineering, NJIT

Dr. Treena Livingston Arinzeh, Committee Member — Date
Professor of Biomedical Engineering, NJIT

Dr. Antje Ihlefeld, Committee Member — Date
Assistant Professor of Biomedical Engineering, NJIT

BIOGRAPHICAL SKETCH

Author: Esma Cetinkaya

Degree: Master of Science

Date: December 2017

Undergraduate and Graduate Education:

- Master of Science in Biomedical Engineering,
  New Jersey Institute of Technology, New Jersey, Newark, 2017

- Master of Science in Medical Physics,
  Istanbul University, Istanbul, Turkey, 2013

- Bachelor of Science in Physics Engineering,
  Gaziantep University, Gaziantep, Turkey, 2009

Major: Biomedical Engineering

“Let the beauty of what you love be what you do."

Rumi

ACKNOWLEDGMENT

First of all, I would like to particularly thank my Thesis Advisor Dr. Mesut Sahin for his patience and support in helping me overcoming numerous obstacles I have faced through my research. Also thanks to my Committee Members Dr. Treena Arinzeh and Dr. Antje Ihlefeld for their guidance and advices during thesis writing stage. I am also grateful to my Graduate Advisor Dr. Max Roman for his understanding and helping me with administrative paperwork. I would also like to acknowledge The Republic of Turkey Ministry of Education for supporting me financially during my Master`s.

Additional my thanks to Neural Prosthetics Lab members, especially Sinan Gok who is actively involved in this study, for their feedback, cooperation and of course friendship. Last, but not the least, I would like to thank my dear mother and entire family for supporting, encouraging, and trusting me during this journey as they have in every stage of my life.

TABLE OF CONTENTS

TABLE OF CONTENTS

(Continued)

TABLE OF CONTENTS

(Continued)

Chapter **Page**

LIST OF TABLES

LIST OF FIGURES

LIST OF FIGURES

(Continued)

LIST OF SYMBOLS

®	Registered
#	Number Sign
≈	Approximately
µm	Micrometer
mm	Millimeter
m	Meter
sec	Second
ms	Millisecond
ºC	Centimeter
mV	Millivolt
Hz	Hertz
kHz	Kilohertz
v/v	Volume/volume
GPa	Gigapascal
MPa	Megapascal
g	Gram
mN	Millinewton
Ω	Ohm

CHAPTER 1

INTRODUCTION

1.1 Objectives

The objective of this thesis is the fabrication and validation of novel carbon fiber microelectrodes for electrophysiological recordings in the central nervous system of experimental animals.

One of the most important goals in neuroscience is to better understand the information processing that takes place in the central nervous system (CNS). Developing devices that can restore neural function lost due to injury or disease is a major goal of the field of neuroprosthetics. The successful implementation of this goal depends on the availability of recording devices that record signals from multiple sites both simultaneously and chronically [1]. These recording devices, microelectrodes, impose two big challenges; the tissue response and the mechanical/electrical stability of electrodes. Even though commercially available microelectrodes are widely used in neuroscience, their limitations like high tissue response and low channel numbers are also well known. Thus, there is a need to develop microelectrodes with improved signal quality, electrode stability, and tissue response. Two key factors that affect all these outcomes are electrode material and size. Among several materials, carbon fiber is one of the most promising electrode materials owing to its strength and flexibility even at micro dimensions.

In this study, we develop a high spatial resolution carbon fiber microelectrode (CFME) bundle, for the spinal cord of rat. Its manufacturing procedure includes simple

fabrication steps and basic equipment, so that this technique can be used readily by others in the field who want to build their own microelectrode. After *in vitro* validation, the CFME bundles were implanted into rats for *in vivo* evaluation. Key outcomes of this study are spikes and tissue displacement. Using three different variants of electrode design, *in vivo* neural recordings were taken in passive versus actively-behaving animals. The recorded electrophysiological signals were then analyzed, to detect single unit spikes. Finally, the tissue displaced by the electrode was demonstrated to be very small using immunohistochemistry.

1.2 Organization

This thesis is divided into five chapters. This chapter presents the objectives and the significance of this work. Chapter 2 reviews the theoretical background for this study. Chapter 3 provides information about the experimental setup and the main components of the design. Chapter 4 shows the results of the preliminary testing using the selected material and techniques. Finally, Chapter 5 presents the conclusion of the work along with the future outlook.

CHAPTER 2

BACKGROUND

2.1 Clinical Significance

Multi-channel electrodes are an important tool for studying neural networks in the CNS. Furthermore, multi-channel electrodes are frequently used as a part of neural prosthetic devices that can help restore sensory-motor function after injury or diseases of the CNS [2]. Spinal cord injury (SCI) in particular leads to paralysis of the skeletal muscles due to trauma during sports or automobile accidents or diseases like ALS [3]. At the moment, there is no treatment that can lead to regeneration of the spinal cord [4].

2.2 Electrophysiology and Neural Activity Recording Techniques

Electrophysiology is the study of the electrical characteristics of cells. These signals are generated by the ionic channels of an excitable cell membrane found in an organ like the heart, the brain or the skeletal muscle. Electrophysiological recordings are taken generally for monitoring the cellular activity or diagnosis. Some of the commonly used electrophysiological techniques are electrocardiography (ECG), electroencephalography (EEG), and electrocorticography (ECoG).

In neuroscience, the signals that are targeted for recording are mainly electrical signals generated by neurons, the excitable cells of the nervous system [5]. Electrophysiological recordings may give information about the neural activity of individual neurons as well as small population of neurons [6]. Particularly, chronic neural

recordings in behaving animals is one of the powerful methods to study neural circuits in the brain to understand functions of its parts [7].

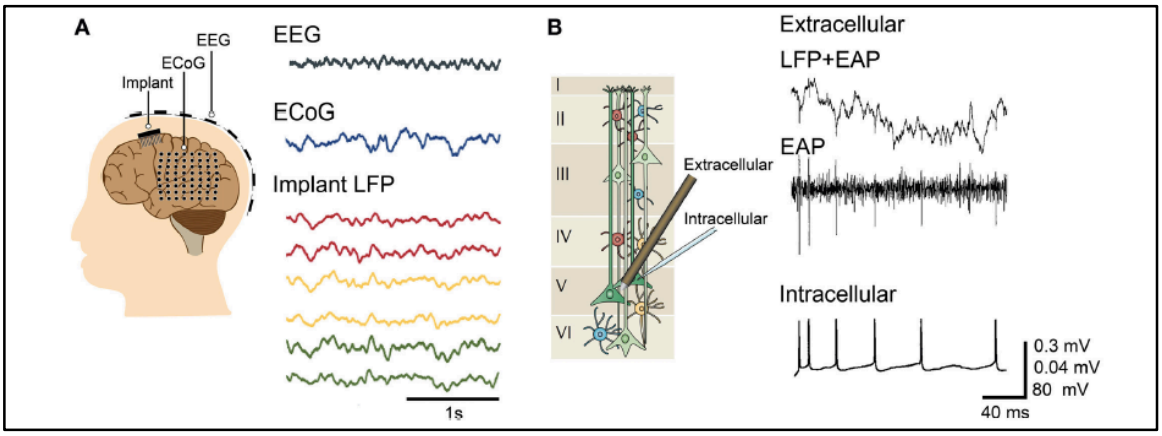

Figure 2.1: Typical electrophysiological methods.

Source: M. E. Obien, K. Deligkaris, T. Bullmann, D. J. Bakkum, and U. Frey, "Revealing neuronal function through microelectrode array recordings," Front Neurosci, vol. 8, p. 423, 2014.

Different electrophysiological techniques used in neuroscience studies are illustrated in Figure 2.1 [6]. From a safety perspective, invasiveness is not desired from a recording modality. However, the closer a recording device is to the signal source, the higher the signal quality is. If we classify the recording techniques according to their invasiveness they can be categorized into three groups. These noninvasive techniques measure the activity of large brain areas in macroscale. In the next group, electrocorticogram (ECoG) is an invasive technique, but the electrodes do not penetrate the brain parenchyma. ECoG electrodes measure more localized activity then EEG electrodes. The multi-electrode arrays (MEAs) are usually implanted into the parenchyma to record extracellular activity from multiple neurons. The recordings collected with ECoG

electrodes and microelectrodes are considered to be at the mesoscale level [6]. Patch-clamp technique measures currents of single ion channels and performs intracellular recordings [6]. Implanted electrodes record extracellular local field potentials (LFP) and extracellular action potentials (AP). LFPs are the summation of excitatory and inhibitory electric signals in the form of currents that are generated from multiple nearby neurons and their processes in a small volume [8].

The amplitude of LFPs is around few hundred micro volts or less. Since signals are very small, it is necessary to amplify them about a thousand times before sampling into a computer. One of the challenges in extracellular neural recording is the background noise. The noise has several components; the intrinsic noise originates from the electronic devices, *e.g.*, the amplifier; the thermal noise is due to the resistive component of the recording electrode, which is calculated using the Boltzmann equation $\sqrt{4kTR\Delta f}$, where R is the resistive component of the electrode impedance, T is the absolute temperature, and Δf is the frequency band of interest; and finally, the biologic component of the noise that is generated from other cells around the electrode.

2.3 Single-Unit and Multi-Unit Recordings

Extracellularly recorded signals contain single action potentials, a.k.a. spikes. When behavioral or physiological events monitored simultaneously with neural activity, correlation between them can be investigated to infer brain functions [9].

Microelectrodes record “spikes” that are generated by membrane currents. These currents flow into the extracellular medium around an excited neuron [9]. If the microelectrode is very small, it can record from a single or relatively small numbers of

neurons [9] and this recording method is called “single-unit recording”. “Unit” in this context means a single neuron. Single-unit recording provides detailed information about characteristic firing pattern of each neuron. Electrode tip size for single-unit recording is in the order of a few micrometers, in the same size scale with the targeted neurons.

“Multi-unit recording” on the other hand, means recording from several units simultaneously [10]. Later these units can be detected by using “spike sorting” technique if the signal-to-noise ratio is sufficiently large [11]. Multi-unit recording method contain more information for neural circuit analysis [9]. Multi-unit recording electrodes are slightly larger than single-unit recording electrodes. When penetrating microelectrodes are used, both single-unit recording and multi-unit recording is possible [3].

2.4 Microelectrodes: Definition, Terminology, Application Areas, History, and Types

If the recording device has several electrodes it is called as a multi-electrode array or a microelectrode array. Microelectrodes are traditionally used for neurotransmitter level detection, pH change detection, drug delivery applications, and recently optogenetic applications. Surface microelectrodes are used in conjunction with optogenetic technique to record signals while stimulating cortex with light [10]. Electrodes used for neurotransmitter level detection, which are also known as neural chemical sensing electrodes, are routinely used in neuroscience studies. They have applications even in human subjects as biosensors [12]. Neural chemical sensing electrodes are also used for neural network studies and can be combined with electrical sensing electrodes. Carbon fiber electrodes have been used widely for neurotransmitter level detection.

Carbon fiber microelectrodes were first introduced in 1979 to measure neurotransmitters [13] and they are still in use as powerful research tools for this kind of applications because of carbon fiber`s unique properties.

Microelectrode technology was first demonstrated in the 1950s [14] and since that time several types of electrode arrays have been developed. The most common types are Michigan shank electrodes, wire electrode arrays, and Utah MEAs. There are companies such as BrainGate, NeuroNexus, Plexon, and Tucker-Davis Technology, which can manufacture these types of electrodes according to customers` needs.

Microelectrodes for electrophysiology applications can be used both for neural recording and stimulating [15]. Recording microelectrodes record electrical activity of neurons in the form of LFPs and spikes [10]. Stimulation electrodes instead stimulates neurons by applying an electric current pulse to the extracellular tissue around the cell [10]. The current should be kept below the safety limits not to cause neuronal damage [15].

The fundamental design principles of all MEAs are 1) enabling high number of recording/stimulation channels from/to nervous system and 2) minimum tissue response [10]. A high channel number increases the spatial precision of recording/stimulation. Tissue safety, electrode longevity, and signal quality are requirements of microelectrode technology and they are strongly correlated with tissue response.

2.5 Microelectrode Design

Simply stated, a microelectrode is composed of a conductive element, insulation material, and a connector. There are intrinsic factors like material properties such as flexibility, conductivity, strength and chemical stability. In microelectrode design, many factors should be taken into account, but there are four essential parameters that are more critical for the electrode quality. They are: the material used for the substrate or shank, insulation material, active electrode site, and electrode geometry.

2.5.1 Electrode Material

Electrode substrate or shank material determines an electrode`s mechanical properties [10]. An ideal electrode material is required to have high conductivity, long-term functional durability, small cross-sectional area, and electrochemical/mechanical stability. Most commonly and traditionally used materials are hard metals like titanium, iridium and their alloys with less brittle metals (e.g. Pt/Ir).

The problems with biocompatibility and tissue damage motivated the research to find noble and safer materials for the electrode substrate. At the present time semiconductors, polycrystalline materials, conductive polymers, and carbon-based materials are receiving more attention because of their superior mechanical properties and suitability for microfabrication techniques. Among these popular materials, carbon fiber is one of the most suitable electrode materials due to its strength, flexibility, and high conductivity. The current microelectrodes suffer from being too rigid compared to the viscoelastic properties of the neural tissue and being too brittle.

2.5.2 Insulation Material

Insulation material on the electrode surface works as a dielectric layer to prevent current leak into the tissue or adjacent conductors. It is also important to limit cross-talk between electrodes in multichannel designs [10]. Cross-talk can disrupt recordings and stimulation. This issue becomes more crucial when designing high spatial resolution electrode arrays because the factors limiting cross-talk (*e.g.,* large distance between electrodes) conflict with high resolution requirements [16].

Some of the insulating materials used are silicon nitride, polyimide, parylene variants, and recently silicon carbide. Epoxies are not suitable since they absorb water. Defects or holes in the electrode coating, delamination, and cracking should be checked before using electrodes. If an electrode`s coated part is exposed in the tissue, a short circuit forms and causes corrosion and failure of the electrode. The thickness of the coating should be sufficient to provide full insulation but on the other hand should be small to prevent the electrode from growing too bulky. The insulating material`s dielectric constant should be small in order not to create large stray capacitances between metallization lines. Also, this material must be biocompatible, and durable.

2.5.3 Electrode Active Area and Desheathing

Exposing an electrode`s active site is also an important step in the electrode fabrication procedure. The point of this step is generating a recording area at the electrode tip by desheathing or removing the coating material on the electrode surface that is used for insulation of the electrode; or deposition of a conductive material. For this process, various techniques such as holding it to a flame [17], blunt blade cut [17], PEDOT (poly(3,4-ethylenedioxythiophene)) deposition [18], and electrode tip coating with various materials

are used by different groups. When choosing a technique, impedance variation, unwanted cracking, and delamination of the coating due to the technique selected should be considered.

The size of the electrode active area determines how selective the electrode is. When the area increases, its selectivity decreases. This means recordings will be the average of a large neuron population, rather than individual neurons. The active area size also affects signal-to-noise ratio (SNR). When an electrode`s active area becomes larger, its impedance decreases and in this case the SNR becomes higher [9]. Contrarily, high impedance values deteriorate the recording capability of electrodes.

2.5.4 Electrode Configuration

Electrode configuration determines how effectively an MEA will stimulate neurons and record signals. High spatial resolution (high channel numbers) increases an MEA`s stimulation and recording capability. Because of this reason high channel numbers are required for many applications. Densely placed electrodes can record from all neurons in a local volume of tissue. At the same time, adjacent channels are required to stay far enough apart to record from distinctive neurons.

Additionally, in the electrode configurations with multiple shanks, staggered electrode lengths help collect data from neurons at different depths. When we consider the layered structure of the nervous system, this feature improves the diversity of information content.

2.6 Microelectrode Target Application Areas

2.6.1 Studies of Neural Circuits

Neurons do not function independently; they are organized and connected in complex networks. These organizations and connections are known as neural circuits [19] or neural networks. They include densely packed synaptic connections, axon terminals, and glial cells. These structures control important functions such as perception, motor function, memory, and learning.

Studying their functions and connectivity helps to identify neural types, understand neural coding and their molecular machinery, and explain their wiring. For that reason, chronic neural recording is an indispensable research tool for the neuroscientist. Understanding the relevant neural circuitry will help to elucidate cognitive, developmental diseases such as Parkinson`s disease, Alzheimer`s disease, and autism, as well as other disabilities due to brain injuries. Consequently, treatment options can be developed.

The reasons for this knowledge gap are the complexity of the brain connections and the difficulties in collecting neural data in awake and behaving subjects. Distinct brain regions are connected to several other regions and they work in concert in any given function. The pathways and firing order changes with every event and activity. Additionally, *in vivo* recording of neural signals with minimal tissue damage is extremely challenging. Particularly when we consider the fact that neurons in the spinal cord have very limited regeneration ability [20], neural damage due to implanted electrodes becomes a much more important issue that prohibits implants in the spinal cord.

2.6.2 Brain-Machine Interfaces

Another popular application for microelectrodes is brain-machine interfaces (BMIs) (or brain-computer interfaces [BCI]). BMI applications have various types and concepts, but in general they are used to record the extracellular electrical activity of neurons for the control of artificial devices. They can provide the control signals for neuroprosthetic devices to restore motor control in paralyzed patients [21]. With BMIs, it is possible to control an artificial limb (Figure 2.2 [21]) or to perform hands-free operation of a cursor with a few motor cortex neurons [22].

Current BMIs suffer from low channel counts and they are able to record only a subset of neurons involved in any brain function. Additionally, tissue damage is still a significant problem for BMIs currently in development.

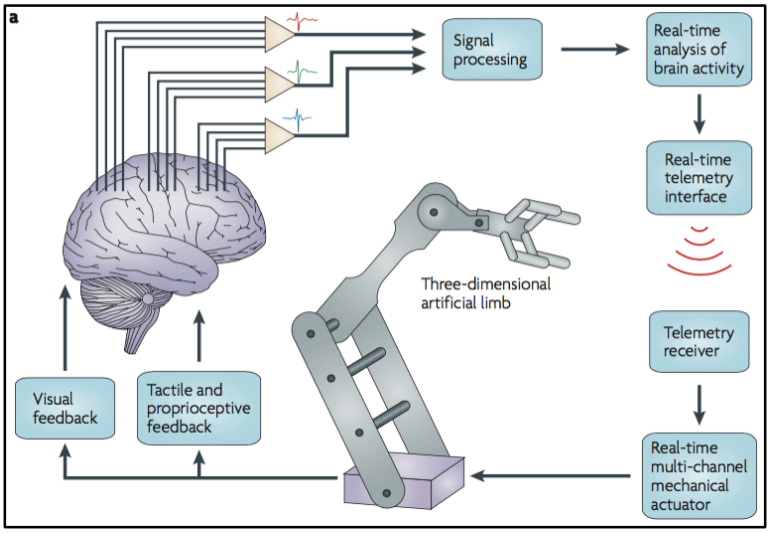

Figure 2.2: Principles of a brain-machine interface.

Source: M. A. Nicolelis and M. A. Lebedev, "Principles of neural ensemble physiology underlying the operation of brain-machine interfaces," Nat Rev Neurosci, vol. 10, no. 7, pp. 530-40, Jul 2009.

BMIs can use different neural activity recording techniques and can be classified according to the invasiveness of the recording technique. For example BMIs with EEG are non-invasive; BMIs with ECoG are considered partially invasive; and BMIs with intracortical microelectrodes are invasive [23].

The main components of BMIs are 1) signal acquisition, 2) feature extraction, 3) feature translation, and 4) device output [24]. These components are basically input (the electrophysiological activity from the subject), output (device commands), and intermediate steps to extract the volitional command from the input [25]. BMIs have applications in communication, environmental control, movement control, and neurorehabilitation [24].

2.7 Carbon Fiber

Carbon fiber is a polymer with long and thin strands. The carbon fibers that are the subject of this thesis are between 5-10 μm in diameter (Figure 2.3 A) [26] B) [27]). It is mainly composed of carbon atoms that have graphite molecular structure. Carbon fiber has a black appearance.

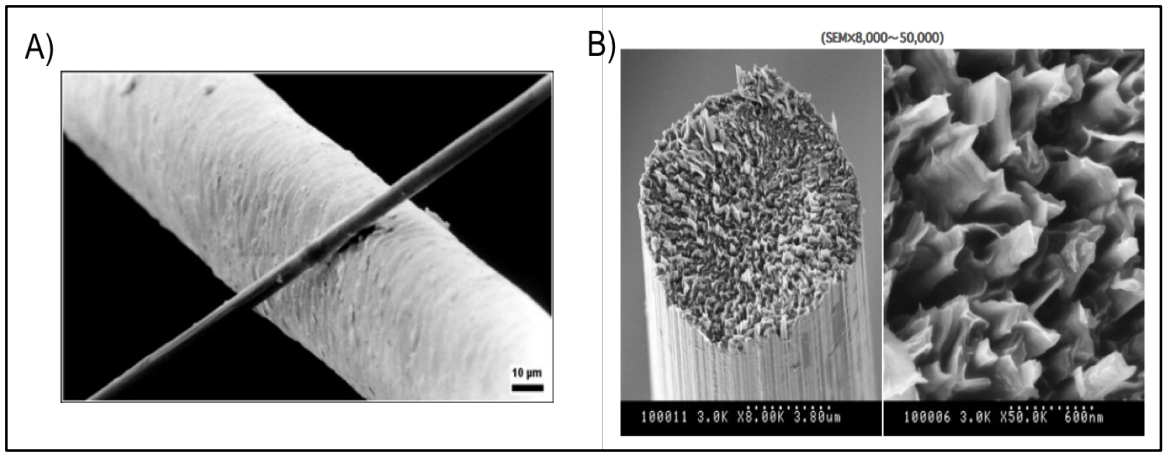

Figure 2.3: Carbon fiber scanning electron microscopy images. A) A 6 μm diameter carbon fiber filament, compared to 50 μm diameter human hair. B) Cross sectional view of a carbon fiber filament.

Source: A) (10/15/2017). File:Cfaser haarrp.jpg (1 October 2005 (original upload date) ed.). Available: https://commons.wikimedia.org/wiki/File:Cfaser_haarrp.jpg B) (10/15/2017). What is carbon fiber? Available: http://www.carbonfiber.gr.jp/english/material/what.html

The raw material used to make carbon fiber is called the precursor. Carbon fibers can be categorized based on precursor material: PAN (polyacrylonitrile)-based, pitch-based, and rayon-based carbon fibers. Among all precursors, PAN is the predominant one because of its various advantages. The preparation of all carbon fiber types includes fibrillation of acrylic resin and heating up to a certain temperature [27]. After the manufacturing, depending on their strength and modulus characteristics carbon fibers can be classified into five groups as seen in the Figure 2.4 [28].

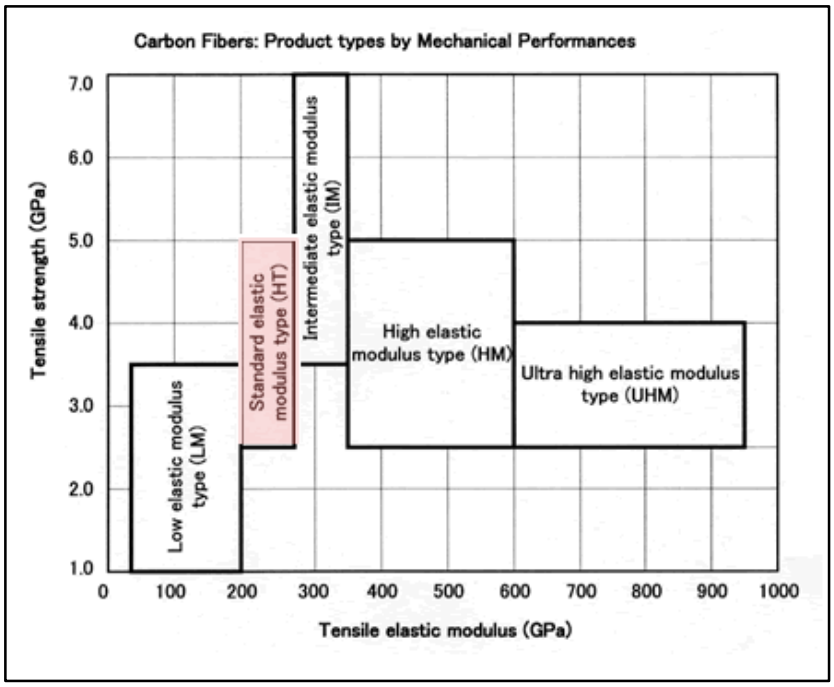

Figure 2.4: Different carbon fiber types based on tensile strength and tensile elastic modulus. Highlighted type is the most commonly used type.

Source: (10/15/2017). Carbon Fiber used in Fiber Reinforced Plastic (FRP). Available: http://www.build-on-prince.com/carbon-fiber.html

One of the unique properties of carbon fiber is its strength. Due to its high tensile strength (average 4 GPa), it does not break easily by forces in the longitudinal direction. This is an advantage for electrode longevity and chronic recordings. It is as much as five-times stronger but at the same time lighter than steel. Because of that, its weight to strength ratio is very small. Handling of even a 7 µm thick carbon fiber filament is possible owing to this property.

Young`s Modulus E (or sometimes Y- tensile elastic modulus in Figure 2.4) is a measure of stiffness for solid materials, and it is calculated as the ratio of stress (force per unit area) to strain (relative change in shape or size); and its SI unit is Pascal (Pa). Carbon fiber`s Young`s Modulus is at the Giga (10^9) Pascal level (approximately 250 GPa for

standard elastic modulus type). This is a very high value compared to most electrode materials (Table 2.1) which indicates its superiority at stiffness. High stiffness is especially important for insertion of thin electrodes into the tissue.

$$E = \frac{\sigma(\varepsilon)}{\varepsilon} = \frac{F \times L}{A \times \Delta L} \tag{1.1}$$

Another parameter for the material property is the bending spring constant "k", which is computed by using the elastic modulus in bending (Young`s Modulus). For the calculation of k, first of all "I", moment of inertia, should be calculated. For neural electrodes with cylindrical beam shape such as carbon fiber electrodes, the formula in given in Equation 1.2.[29] to calculate the inertia constant. For a rectangular prism shape like traditional electrodes inertia constant can be calculated with the formula in Equation 1.3 [29] and substituted in Equation 1.4 to find the spring constant. In these formulas, r is the radius, w is the width, t is the thickness, and l is the length.

$$I = \frac{\pi r^4}{4} \tag{1.2}$$

$$I = \frac{wt^3}{12} \tag{1.3}$$

$$k = \frac{3EI}{l^3} \tag{1.4}$$

Table 2.1: Physical Properties of Various Probe Designs

Electrode Material	*E (MPa)*	*k (mN/m)*	*Length (mm)*	*Thickness (µm)*	*Width (µm)*
Tungsten	390,000	44,868	2	N/A	50 (diameter)
Carbon Fiber	241,000	0.61	5	N/A	6.8 (diameter)
Silicon	165,000	136.99	3	100	123
Parylene-c	3,778	94.5	2.5	25	100
Open Architecture Parylene-c	3,778	0.26	1.1	5	4
Polyimide	2,800	265.48	1.5	20	160

Source: P. R. Patel, "Carbon fiber microelectrode array for neuroprosthetic and neuroscience applications," Doctorate, Biomedical Engineering, The University of Michigan, Michigan.

Carbon fiber`s high strength, stiffness, and mechanical/chemical resistance make carbon fiber very popular in several areas [30]. Its chemical resistance also contributes to an electrode`s longevity and reduce tissue response.

On the other hand, its cost is high because mass production is not possible and demand for carbon fiber is still limited. A disadvantage is regarding its health hazard. Since carbon fiber is very light and tiny, it can circulate in the air and can be inhaled easily [31].

2.8 The Spinal Cord

The spinal cord is a part of the nervous system and connects the brain to the body. The spinal cord is comprised of a bundle of nerves which extend from the brain`s base to the lower back part of the body. Human spinal cord is about 45 cm long and 1.2 cm thick while the rat spinal cord`s cervical part is about 10 mm long and 4 mm thick (for Long Evans rat) (Figure 2.5 [32]).

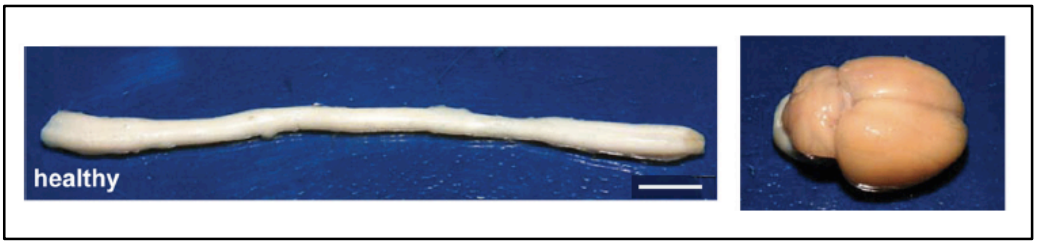

Figure 2.5: Long Evans rat spinal cord. Scale bar is 10 mm.

Source: R. Fairless et al., "Preclinical retinal neurodegeneration in a model of multiple sclerosis," J Neurosci, vol. 32, no. 16, pp. 5585-97, Apr 18 2012.

The spine is formed of a series of bones called “vertebrae”. Both human and rat vertebral column has 7 of cervical vertebrae (the number of cervical spinal nerves is 8). The spinal cord is surrounded by layers called meninges (the dura mater, the arachnoid, and the pia mater) in continuum with the brain (Figure 2.6 [33]).

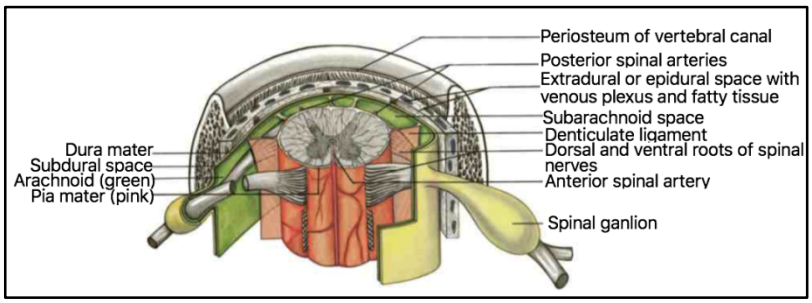

Figure 2.6: Meningeal covering of the spinal cord (anterior aspect) (schematic drawing).

Source: C. Y. Johannes W. Rohen, Elke Lutjen-Drecoll, Color atlas of anatomy, 7th Edition ed. Wolters Kluwer, Lippincott Williams & Wilkins.

Corticospinal tract (CST) is one of the descending pathways of the nervous system. Corticospinal projection is the most direct pathway between the cerebral cortex and spinal motor neurons. The CST is responsible for the fine movements like that of the fingers.

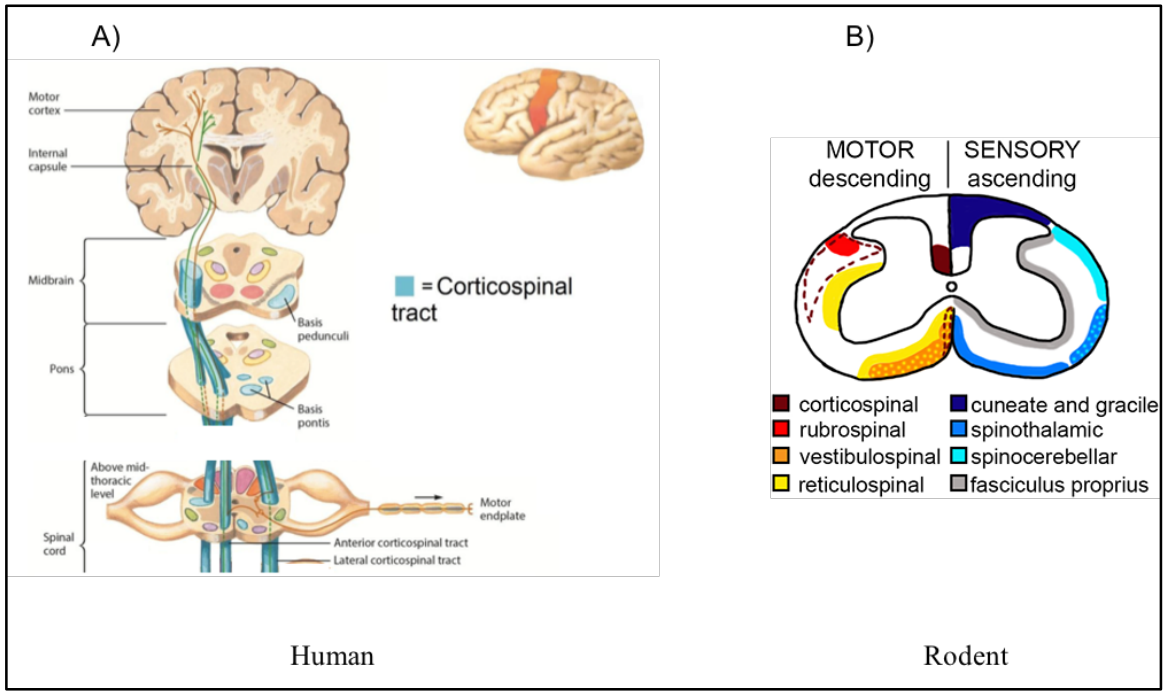

Figure 2.7: Human versus rodent corticospinal tract.

Source: A) P. M. Roos, "Studies on metals in motor neuron disease," Institute of environmental medicine, Karolinska Institutet, Stockholm, 2013. B) C. F. Vogelaar and V. Estrada, "Experimental Spinal Cord Injury Models in Rodents: Anatomical Correlations and Assessment of Motor Recovery," in Recovery of Motor Function Following Spinal Cord Injury, 2016.

The CST neurons (also known as upper motor neurons) have big pyramid-shaped somas in the 5th layer of the motor cortex. In humans, most of the corticospinal axons in the spinal cord cross the midline and enter the lateral column of the white matter [34]. The location of the CST in the spinal cord varies among species. In rodents, it is located in the

dorsal column of the spinal cord whereas it is in the dorsolateral funiculus in humans (Figure 2.7 A) [35] B) [36]).

2.9 Previous Carbon Fiber Microelectrode Studies

Carbon fiber microelectrode (CFME) technology started with Armstrong-James Michael *et al.* in 1979 [37]. He is the first researcher who demonstrated the ability of extracellular neural activity recording of carbon fibers. This design had a triple barrel structure with glass insulation on the fibers. The recordings were performed by exciting neurons with glutamate. In 2010, Budai *et al.* developed a similar design with more barrels and recorded spikes [38].

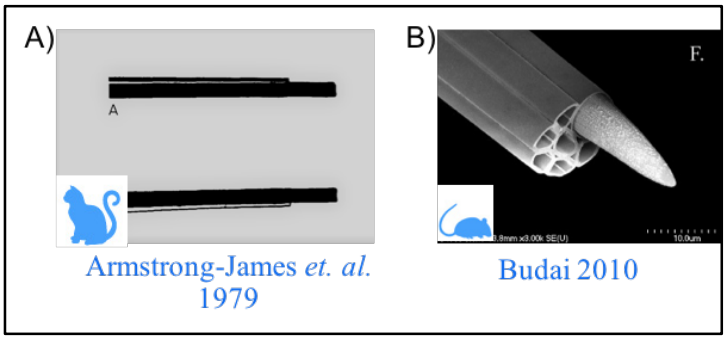

Figure 2.8: Previous single channel carbon fiber electrodes.

Source: A) J. M. Armstrong-James Michael, "Carbon fibre microelectrodes," Journal of Neuroscience Methods, vol. 1, pp. 279-287, 1979. B) D. Budai, "Carbon fiber-based microelectrodes and microbiosensors," in Intelligent and Biosensors, vol. January 2010, V. S. Somerset, Ed., 2010.

The first *in vivo* extracellular activity recording CFMEs with multichannel feature was developed by Piironen in 2011 [39]. His design had tetrode shape electrodes and he used them for acute recordings in the brain of a blowfly. In 2012, Kozai *et. al.* recorded

signals from the motor cortex of rats for 5 weeks with microthread shaped electrodes [40]. In 2013, Guithchounts *et. al.* established a 16-channel microthread electrode bundle and recorded signals from the premotor nucleus HVC of birds for approximately one year [17]. Finally, in 2015 Patel *et. al.* recorded signals more than 100 days from the motor cortex of rats with a 16-channel array shaped microelectrode [41] (Figure 2.9).

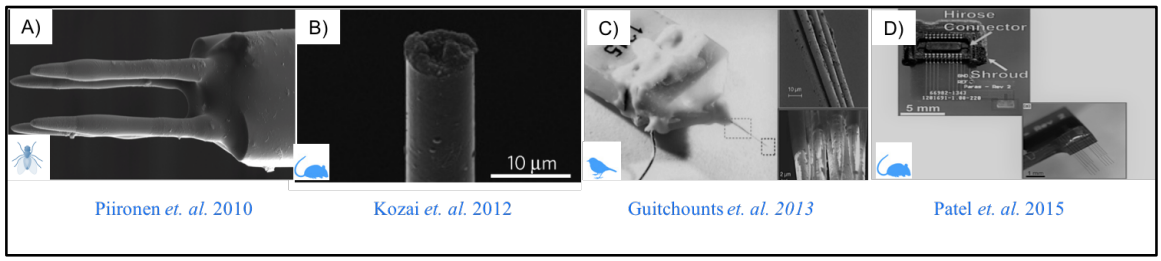

Figure 2.9: Previous multiple channel carbon fiber electrodes.

Source: A) A. Piironen, M. Weckstrom, and M. Vahasoyrinki, "Ultrasmall and customizable multichannel electrodes for extracellular recordings," J Neurophysiol, vol. 105, no. 3, pp. 1416-21, Mar 2011.B) N. B. L. Takashi D. Yoshida Kozai, Paras R. Patel, Xiaopei Deng, Huanan Zhang, Karen L. Smith, Joerg Lahann, Nicholas A. Kotov & Daryl R. Kipke, "Ultrasmall implantable composite microelectrodes with bioactive surfaces for chronic neural interfaces," Nature Materials vol. 11, pp. 1065-1073, 2012. C) G. Guitchounts, J. E. Markowitz, W. A. Liberti, and T. J. Gardner, "A carbon-fiber electrode array for long-term neural recording," J Neural Eng, vol. 10, no. 4, p. 046016, Aug 2013. D) P. R. Patel et al., "Insertion of linear 8.4 mum diameter 16 channel carbon fiber electrode arrays for single unit recordings," J Neural Eng, vol. 12, no. 4, p. 046009, Aug 2015.

CHAPTER 3

METHODS

3.1. Overall Study Organization

In this study, two different designs of carbon fiber microelectrodes were fabricated: first one has only single blunt cut carbon fibers (n=32) and second one has three variants (single blunt cut carbon fibers (n=6), single desheathed tip carbon fibers (n=16), and triple blunt cut carbon fibers (n=10)). After validation with *in vitro* tests, they were implanted into the spinal cord of two Long Evans rats (male, 350-375 g) and neural signals were recorded during awake conditions. After one month of survival time, both animals were sacrificed and the electrode`s footprint in the tissue was evaluated by immunohistochemistry. Lastly, recorded signals and *in vivo* electrode impedance measurements were analyzed. Figure 3.1 shows the overall organization of the study.

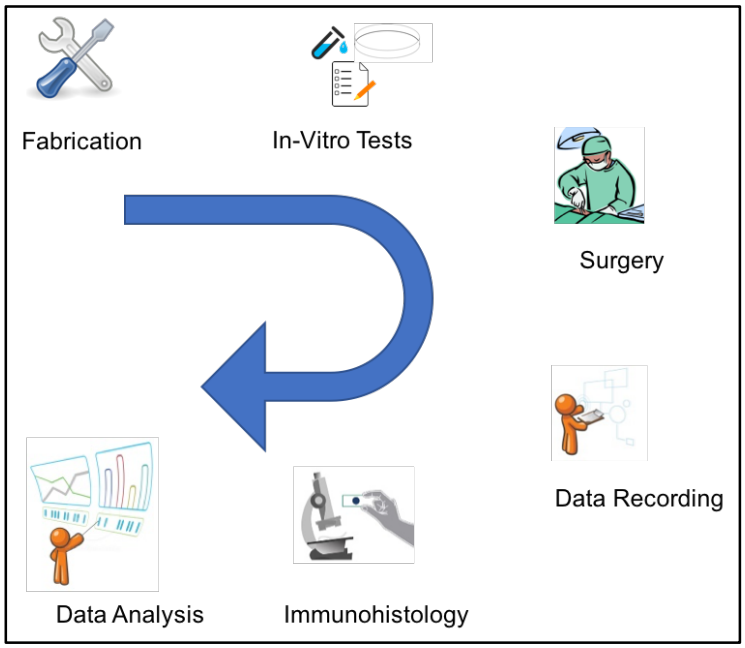

Figure 3.1: The study organization.

3.2 Main Components

3.2.1 Carbon Fiber

Seven micrometer diameter carbon fibers (Goodfellow Cambridge Ltd., England) were separated by curing at around 400˚C degree for 5 hours to remove epoxy from their surface. Carbon fiber filaments were separated individually and anchored on a frame to prepare for the coating process. Then they were sent to Specialty Coating Systems in Indianapolis to receive 0.76 µm parylene-C coating at room temperature.

3.2.2 The Connector

For this study, a neuro nano strip pin type connector (A79026-001) (Omnetics Connector Corporation, Minneapolis) was used (Figure 3.2).

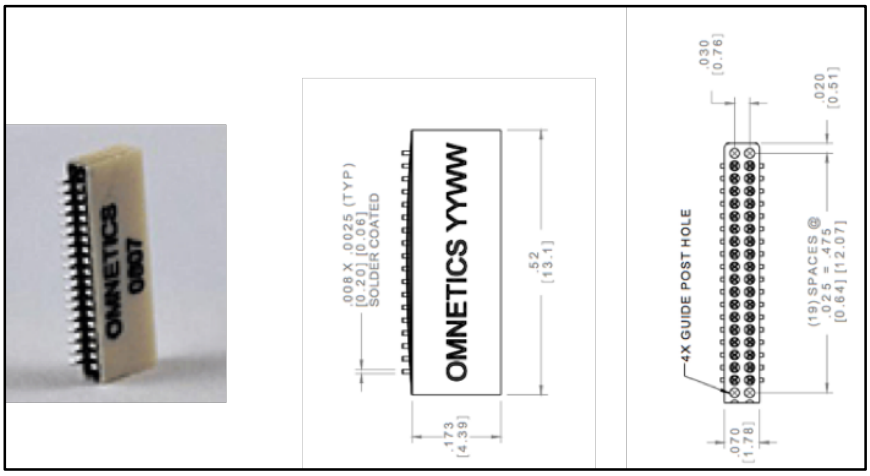

Figure 3.2: Omnetics connector used in the current study.

Source: http://www.omnetics.com/products/neuro-connectors/nano-strip-connectors?page1016=1&size1016=12.

3.3 Fabrication of CFME Bundles

3.3.1 The First Design

Thirty-two carbon fiber filaments were cut to a length of 3.5 cm. Under microscope approximately 200 µm length coating was removed from one ends of the filaments by using a soldering iron heated up to 280˚C. Each filament was connected to a separate pin on the micro-connector using conductive silver epoxy (EpoTek, MA) (Figure 3.3 C)).

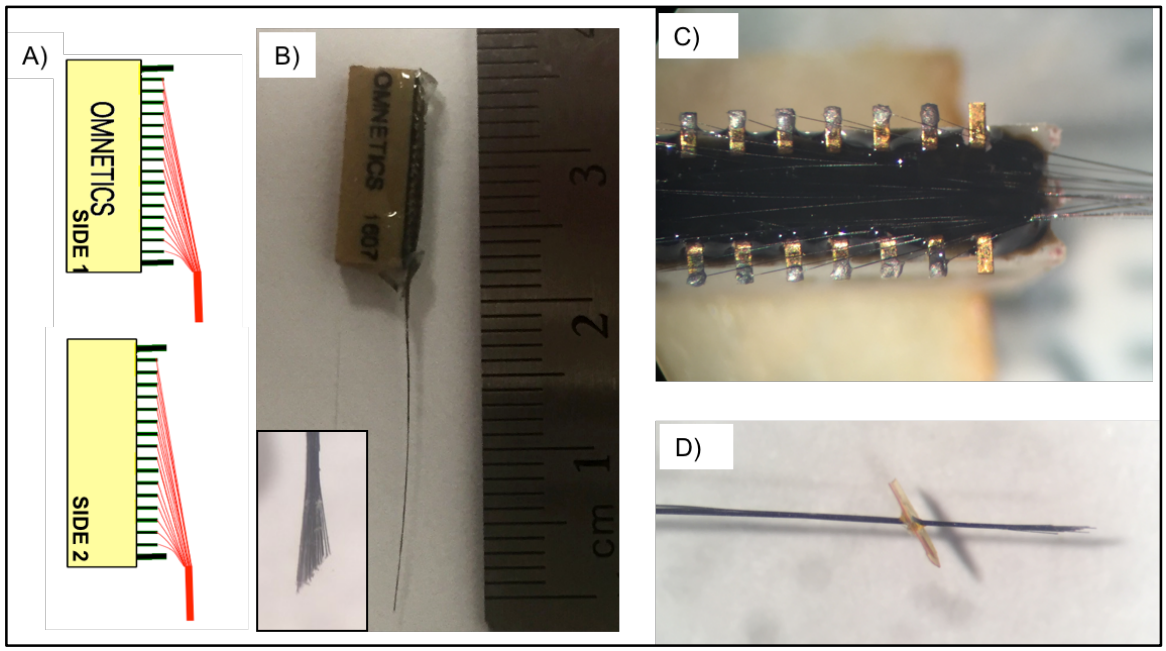

Figure 3.3: The first design CFME. A) The first design CFME bundle`s illustrative image which has single blunt cut carbon fiber filaments. B) The CFME bundle and its staggered shape tip. C) Top view which shows connections between contacts and carbon fiber filaments. D) A polyimide attachment at the tip of the bundle.

The other ends of the filaments were cut into a staggered shape with a surgical blade at 2.5 cm from the connector (Figure 3.3 B) detailed view). The channels were secured and insulated by using clear medical epoxy (OJ 2116 EpoTek, MA). A small amount of medical

epoxy was applied to the middle of the electrode length to keep the fibers together as a bundle.

3.3.2 The Second Design

A plain non-conductive printed circuit board (PCB) was placed between two rows of the connector pins. The proximal ends of the filaments were desheathed with soldering iron as described above. Carbon fiber filaments were connected to the pins individually with silver epoxy in half the channels. Ten channels on one side of the connector had triple carbon fiber filaments at each contact side.

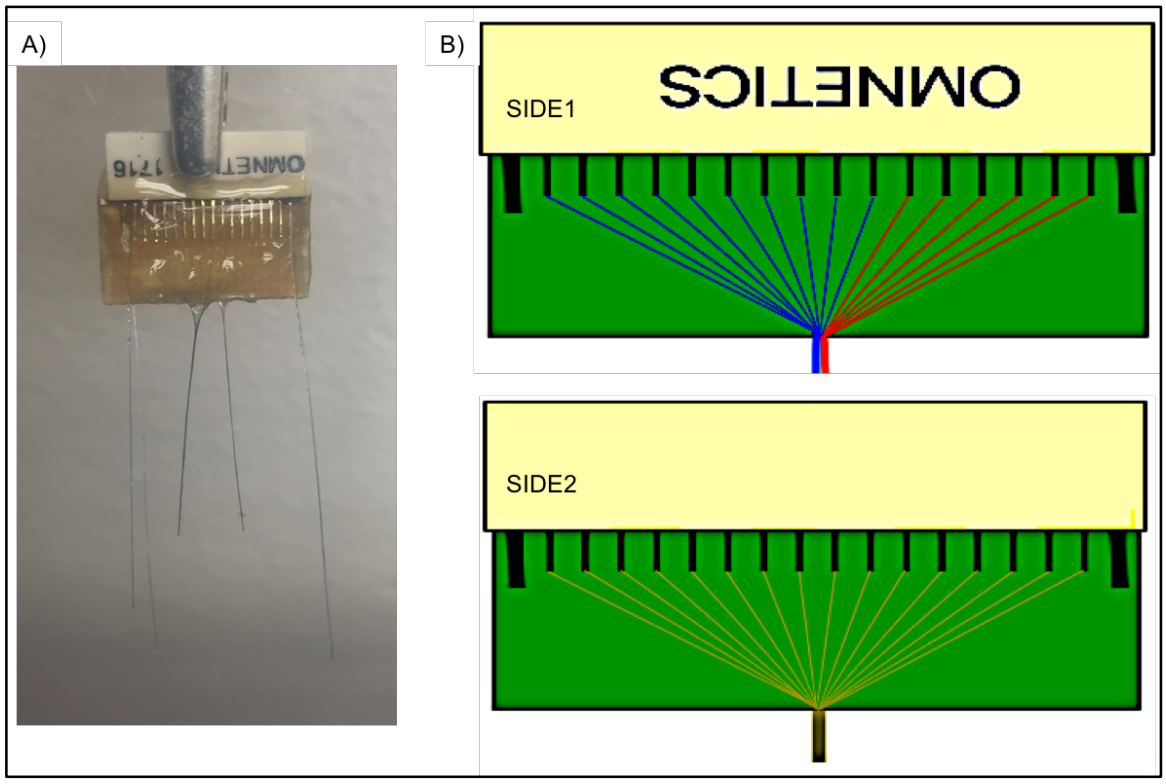

Figure 3.4: The second design CFME. A) A picture of the second design CFME bundle. B) Its illustrative drawings. There is 10 triple blunt cut and 6 single blunt cut carbon fiber filaments on side 1 and 16 single and desheathed filaments on side 2.

Electrodes from each side of the PCB were gathered into a separate bundle, and each bundle was compromised of 16 channels (Figure 3.4). Two of the upper corner pins were used as reference electrodes that are made from Teflon-coated multi-strand stainless steel wires (50 microns diam.). The connector contacts were secured and insulated with medical epoxy. The other ends of the filaments were cut into staggered shape with a surgical blade at 2 cm from the PCB. Again, a small amount of medical epoxy was applied at the middle along the electrode bundles and a piece of polyimide film (25μm thick) was glued 1.5mm from the fiber tips to mark the length that will be inserted into the spinal cord. Fiber tips in one of the bundles were desheathed about 75 μm of its length using a technique that was developed as a part of this study as detailed in the next section below.

3.4 Desheathing Electrode Tips

For this study, a system was developed for desheathing fiber tips with parylene-C coating. The advantage of this technique is that it is possible to remove the coating material in a controlled manner at the desired length without damaging the carbon electrodes.

This system is based on electrical heating and works like a micro oven to increase the local temperature at the electrode tip (Figure 3.5). Briefly, it is comprised of a simple circuit, a stainless steel hollow tube, and a thermocouple.

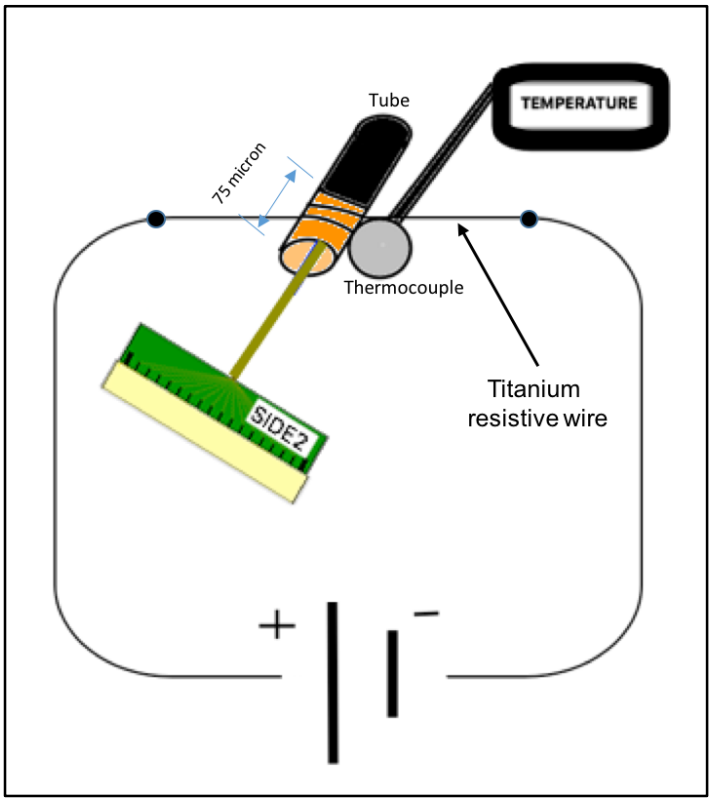

Figure 3.5: The desheathing system.

The resistance wire is wrapped around the metal tube a few times. The metal tube`s hollow part is 75 µm deep from the tip opening. The thermocouple under the tube monitors the temperature of the chamber. The tip of carbon fiber bundle on the side 2 of the second design was inserted into the metal tube. The current passing through the resistance wire was adjusted so that the temperature reaches up to 290°C. Carbon filaments were left in the chamber for 2 minutes while the current is kept on to completely remove the parylene-C coating at the carbon fiber tips.

3.5 *In vitro* Tests

3.5.1 Bubble Test

This test is performed by applying a small DC anodic current from a 9 V battery in a conductive solution (Dulbecco`s Phosphate Buffered Saline [DPBS] [Ge Healthcare Life Sciences]) to determine if the tips are exposed and the rest of the fiber is insulated. The circuit includes the CFME bundle, a reference electrode, the PBS solution in a Petri dish, a 9 V battery, and a 40-100 kΩ resistance. Electrolysis of water occurs at the exposed parts of the carbon fiber and gas bubbles form when the circuit is closed allowing a small current to pass through the electrode into the solution.

Under 100x microscope, the entire lengths and tips of electrodes were inspected. Ideally, it is expected to observe bubbles only at the tip of an electrode which confirms that the deinsulation was done successfully and the electrode is functioning. Bubbles on the parylene-C coated parts of the electrode surface indicate coating defects.

3.5.2 Impedance Test

This test was performed also in PBS. For this experiment an analog impedance meter (Bak Inst.) was used to measure the electrode impedances at 1 kHz against a large reference electrode. Impedance values were expected to decrease after desheathing of parylene-C coating.

3.5.3 Scanning Electron Microscopy (SEM) Imaging

SEM images were taken at NJIT's Otto H. York Center for Environmental Engineering and Science. The purpose of SEM imaging was to check the intactness of the coating material, and verify the desheathing technique and the exposed area of the electrodes.

3.6 Surgery

Two Long Evans rats were used in this study. The surgery procedure briefly: The animals` back skin was shaved and the animal was anesthetized with 5% isoflurane (v/v). Its head was mounted to the stereotaxic frame. Anesthesia was maintained at 1-3 % isoflurane during surgery. Animal vitals were monitored with a pulse-oximeter and a rectal temperature probe. Ointment was applied to the animals` eyes to keep them from drying. A dorsal laminectomy at the cervical level was performed to assist the resection of the dura for exposing the pia. The electrode bundle of the first design was inserted vertically along the central fissure of the spinal cord of the first rat into the dorsal column at the C4 level. Both electrode bundles were implanted to the same location in the second rat as well.

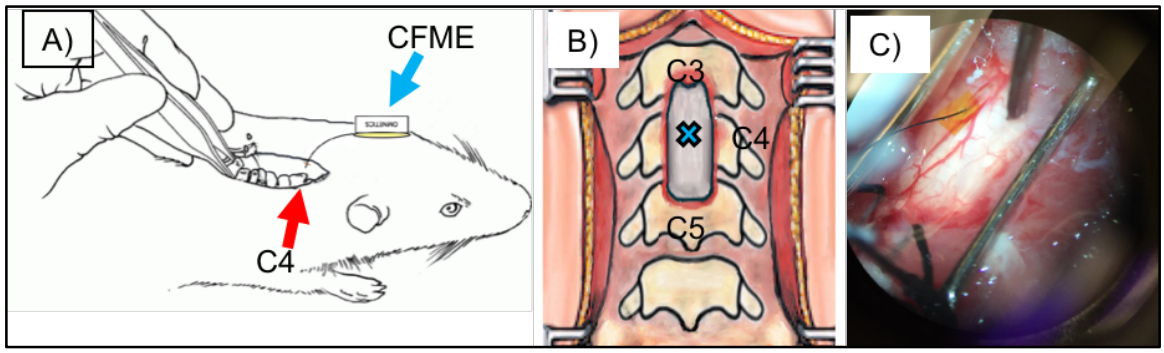

Figure 3.6: Surgery A) The laminectomy. B) An illustrative figure which shows top view of the surgical area. C) A picture of the implantation area.

In both cases, the bundles were inserted for 1.5 mm of their length, using the guidance of the polyimide attachment. Then bundles were secured in place by applying a small amount of cyano acrylic glue on the pia. A metal frame was placed on the spinal cord by tying it to C2 and C5 vertebral bones with 4.0 silk sutures. The Omnetics connector was

attached to the frame with dental acrylic. The connector was protruding half-way through the skin for making connection with the multi-channel neural amplifier. Each microelectrode bundle had some slack to avoid any pulling on the spinal cord. Finally, the skin incision was closed with absorbable sutures.

3.7 Data Recording

Neural signals were recorded using a multichannel amplifier (Ripple, UT) with a front end headstage (Ripple Grapevine, UT), and MATLAB (Mathworks, Inc.) (Figure 3.7).

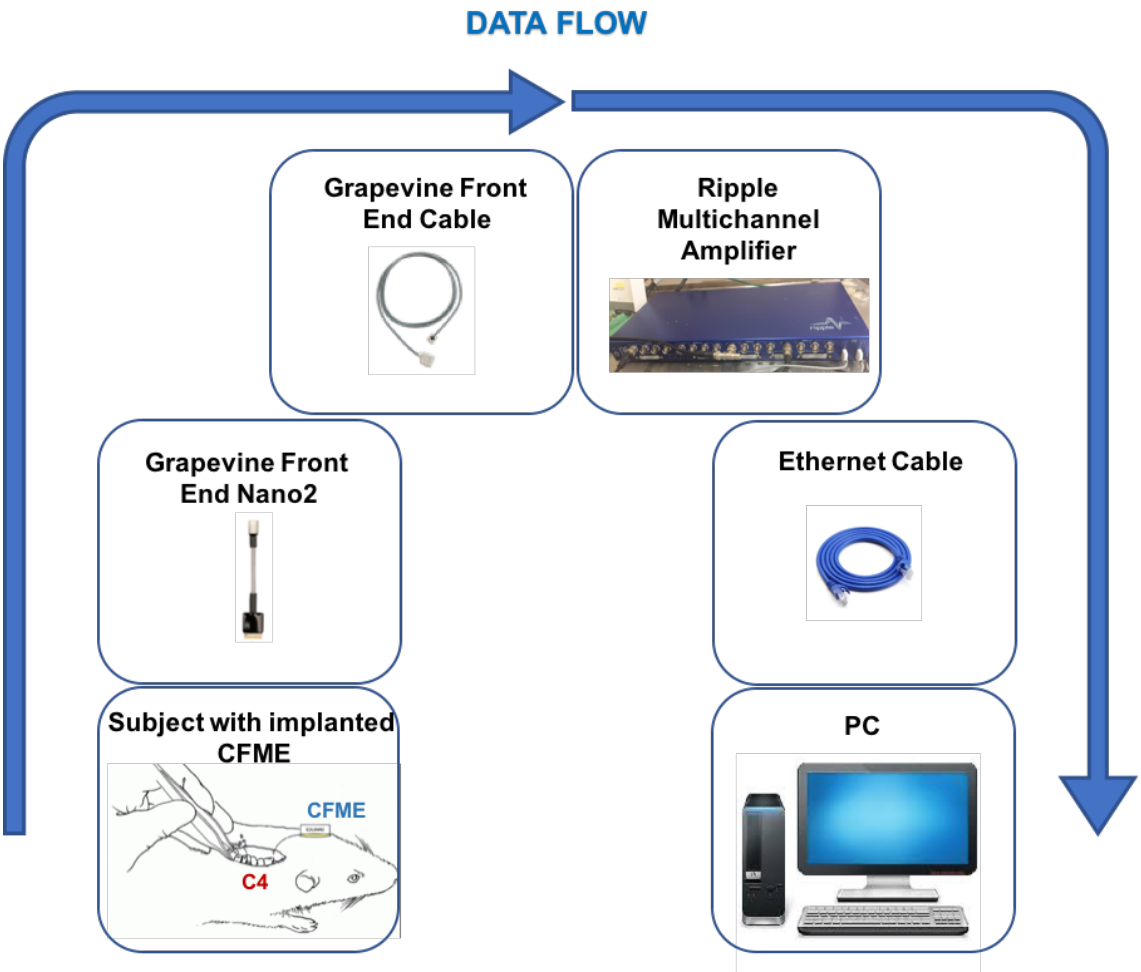

Figure 3.7: Data flow.

The animals` movements were captured by a video camera to monitor and document their state (awake/anesthetized; active/quiet). Special attention was given to the signals taken during face cleaning since this task involves cyclic forelimb movements and does not require training [42]. Also, *in vivo* impedance values were measured before each session.

3.8 Histology

At the end of 4-week survival period both animals were sacrificed. The CFMEs and the implanted sections of the spinal cords were extracted. The bundles of the CFMEs were cut at the point that they enter the spinal cord. After perfusion, the cut ends of the carbon fibers in the tissue were removed. This method prevented damaging the tissue encapsulation layer around the electrode while removing them.

The first rat`s transverse sections were sliced to a thickness of 15 μm and then stained with antibodies of LFB (Luxol Fast Blue) for myelin, H&E (Hematoxylin) for nuclei, and Eosin.

3.9 Data Analysis

3.9.1 Neural Signal Analysis (Rat #1)

Signal processing was performed in MATLAB. The specific aim for this experiment was to show spike activity. To this end, raw data from three sessions that consisted of multiple trials of 32-channel recordings were filtered in MATLAB. Channels that had the best *in vitro* test results were selected. Animal behaviors during each trial was evaluated and the quiet and face cleaning episodes were extracted. Spikes were detected and raster plots were

drawn. Firing rates for the selected trials and channels were analyzed. Spikes were clustered based on their amplitude and width, and signal-to-noise ratios (SNRs) were calculated.

3.9.2 Neural Signal Analysis (Rat #2)

The particular goal of this experiment was to determine how *in vivo* impedance values and spike counts change according to the desheathing of carbon fiber tips and the number of carbon fiber filaments attached on individual channels. The channels with these conditions were compared to control channels which had a single carbon fiber filament with a blunt cut end. Comparative analysis was done in terms of impedances, spike counts, and SNR values for each group.

- Group 1 (control group): single filament with blunt cut ends
- Group 2 (triple filaments): three carbon fiber filaments with blunt cut ends
- Group 3 (desheathed filaments): single carbon fiber filament with desheathed tips

CHAPTER 4

RESULTS

4.1 SEM Images

Three carbon fiber filaments were analyzed by SEM images: an uncoated carbon fiber with blunt cut, a coated carbon fiber with blunt cut, and a coated carbon fiber with desheathed tip. The images on the left panel of Figure 4.1 belongs to an individual carbon fiber filament. Its thickness was measured as 6.24 µm approximately.

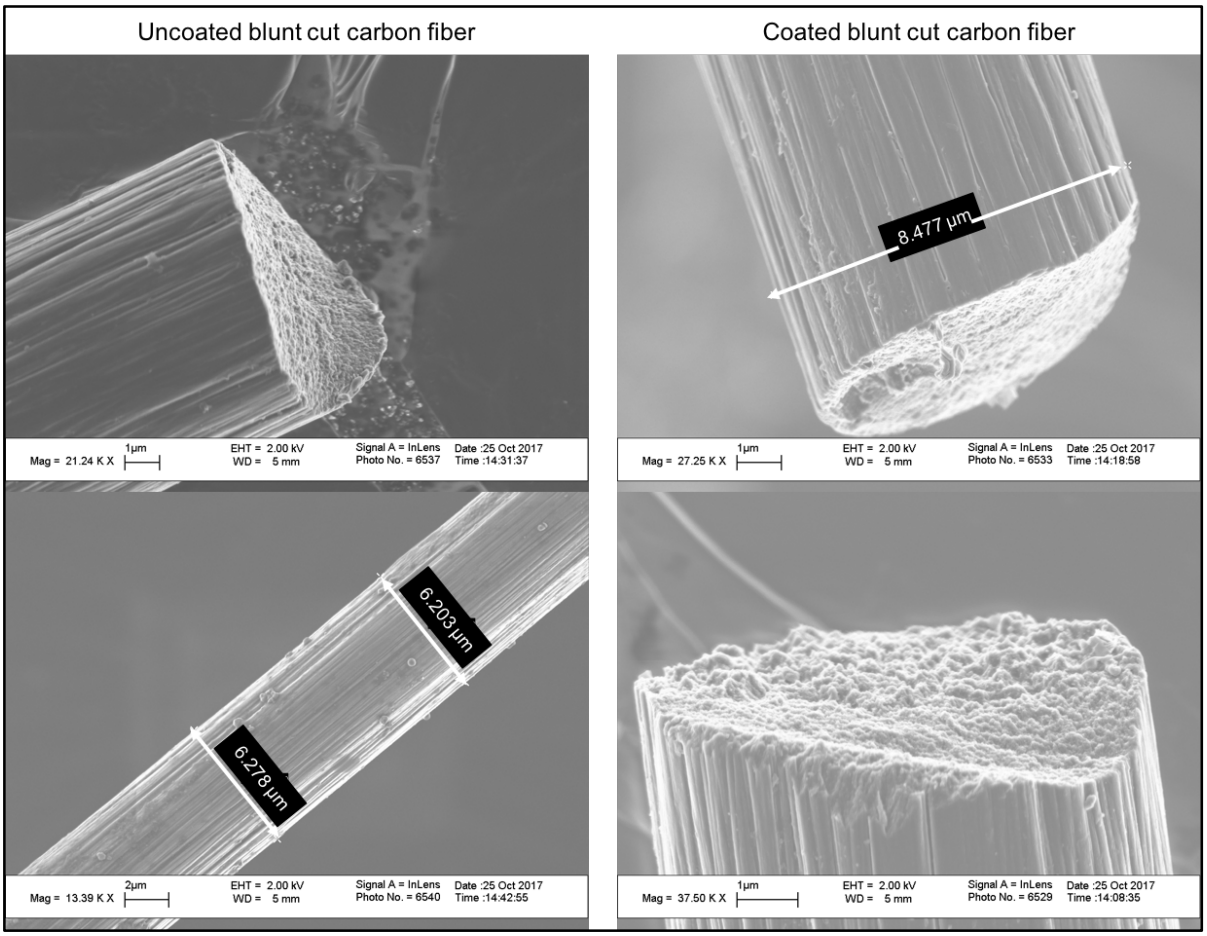

Figure 4.1: SEM images of uncoated blunt cut carbon fiber and coated blunt cut carbon fiber.

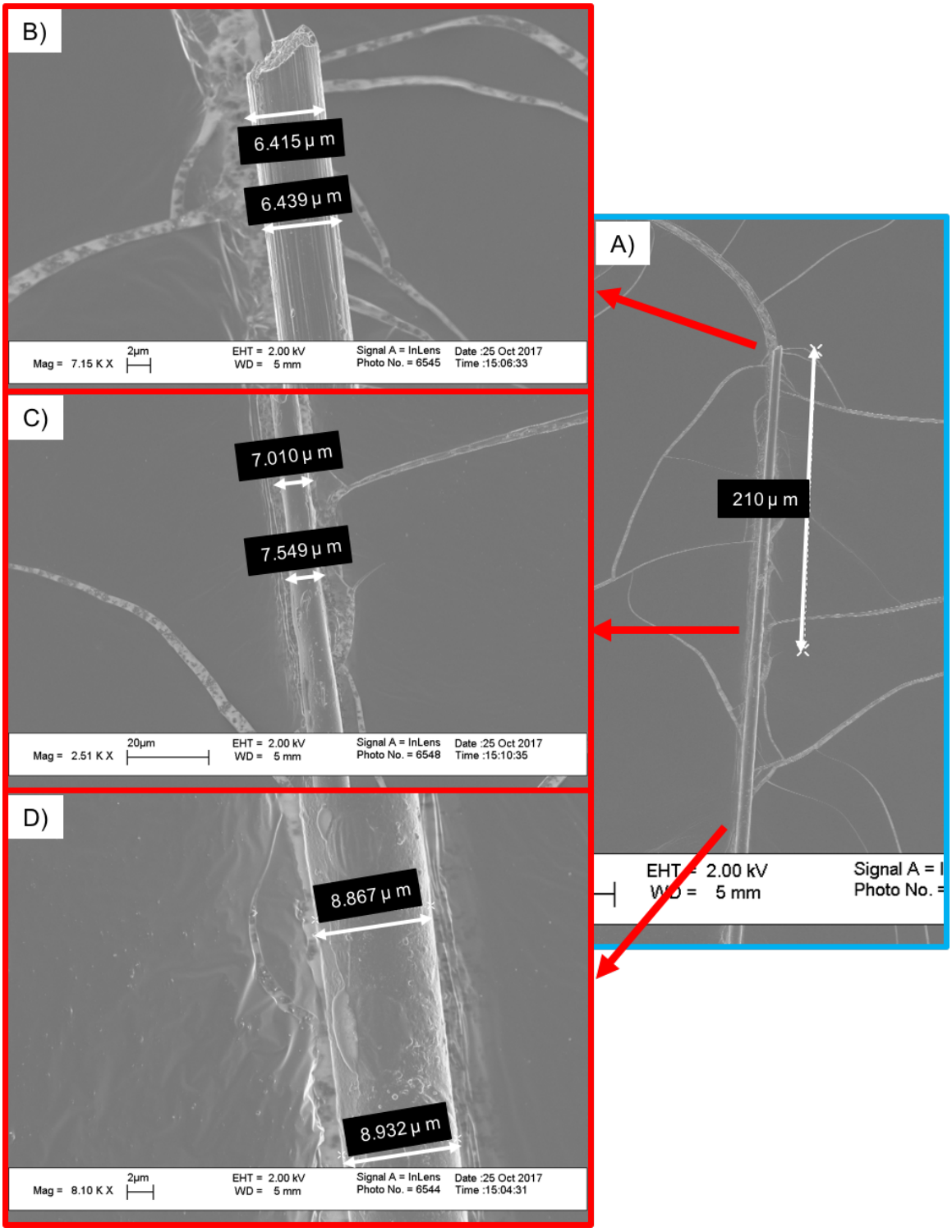

Figure 4.2: SEM images of soldering iron desheathed carbon fiber. A) shows the entire desheathed length. The thickness measurement at the tip is approximately 6.42 µm (B), at the end of desheathing length the average is 7.28 µm (C), and at the remaining part of the carbon fiber filament it is 8.90 µm (D).

Other two images on the right panel shows the structure and the thickness (8.47 μm) of another carbon fiber filament with parylene-C coating. Both panels also depict the results of blunt cutting.

The SEM images in Figure 4.2 confirms that desheathing with soldering iron was effective but not uniform along the entire desheathed length.

4.2 The Results from Rat#1

4.2.1 *In vitro* Bubble and Impedance Tests of The Electrode

Table 4.1: Impedance and Bubble Test Results

Channels	Bubble Test	Impedance Test	Channels	Bubble Test	Impedance Test
1	√	In the range	17	√	In the range
2	x	In the range	18	x	N/A
3	x	N/A	19	x	N/A
4	√	In the range	20	x	N/A
5	√	In the range	21	x	N/A
6	√	In the range	22	x	In the range
7	x	N/A	23	x	In the range
8	√	In the range	24	x	In the range
9	x	N/A	25	x	In the range
10	x	N/A	26	√	In the range
11	x	N/A	27	√	In the range
12	x	N/A	28	√	In the range
13	x	In the range	29	x	In the range
14	x	N/A	30	√	In the range
15	√	In the range	31	√	In the range
16	x	N/A	32	√	In the range

Bubble and impedance tests were performed twice. The channels that passed all four tests were included in further analysis (green channels in the Table 4.1).

Good Channels: 1, 4, 5, 6, 8, 15, 17, 26, 27, 28, 30, 31, and 32.

4.2.2 Neural Signals

Neural signals were first filtered with a 4th order butterworth bandpass filter (100-1500 Hz) in MATLAB.

Session #1:

The signals in Figure 4.3 show how signals on one channel change during different states of the animal.

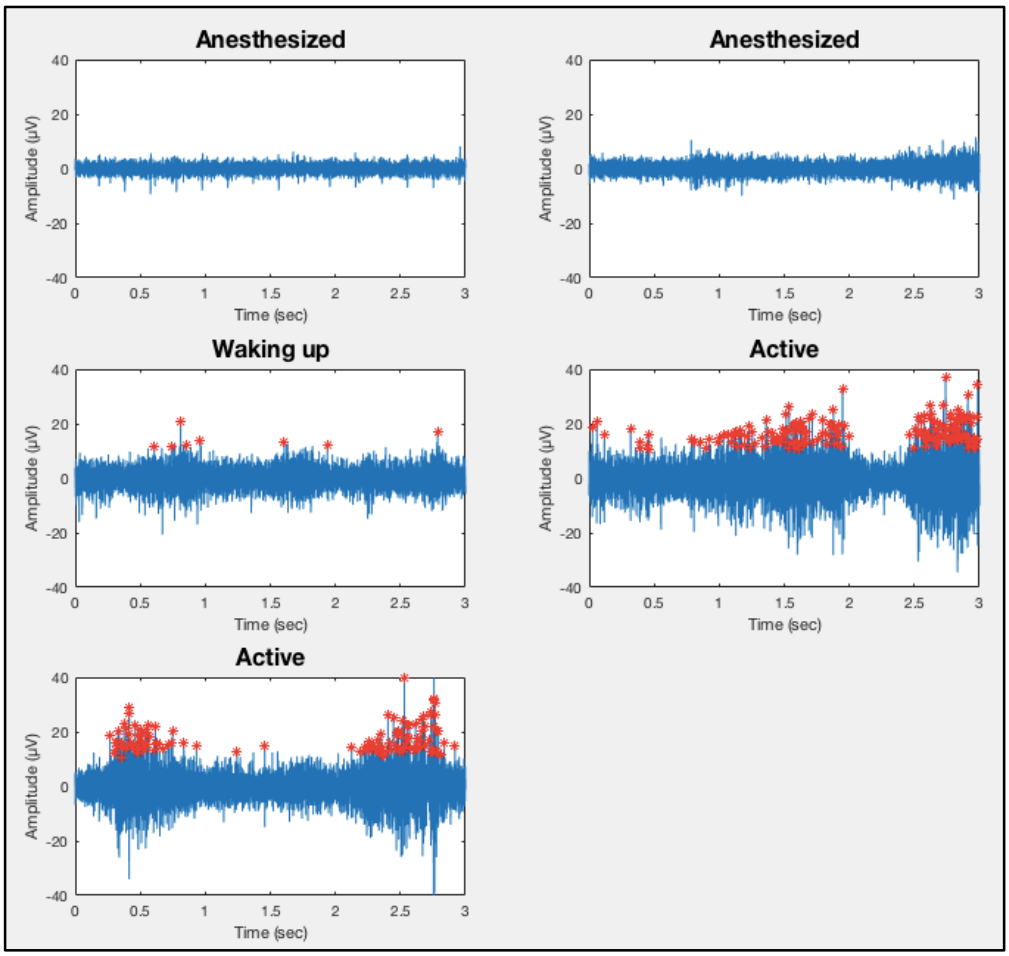

Figure 4.3: Spike activity change with animal state (channel:1; trials:1, 12, 14, 21, and 22).

Session #2:

Figure 4.4 shows the spikes detected on one of the good channels during animal`s awake state. The average amplitude of the signals is 150 µV.

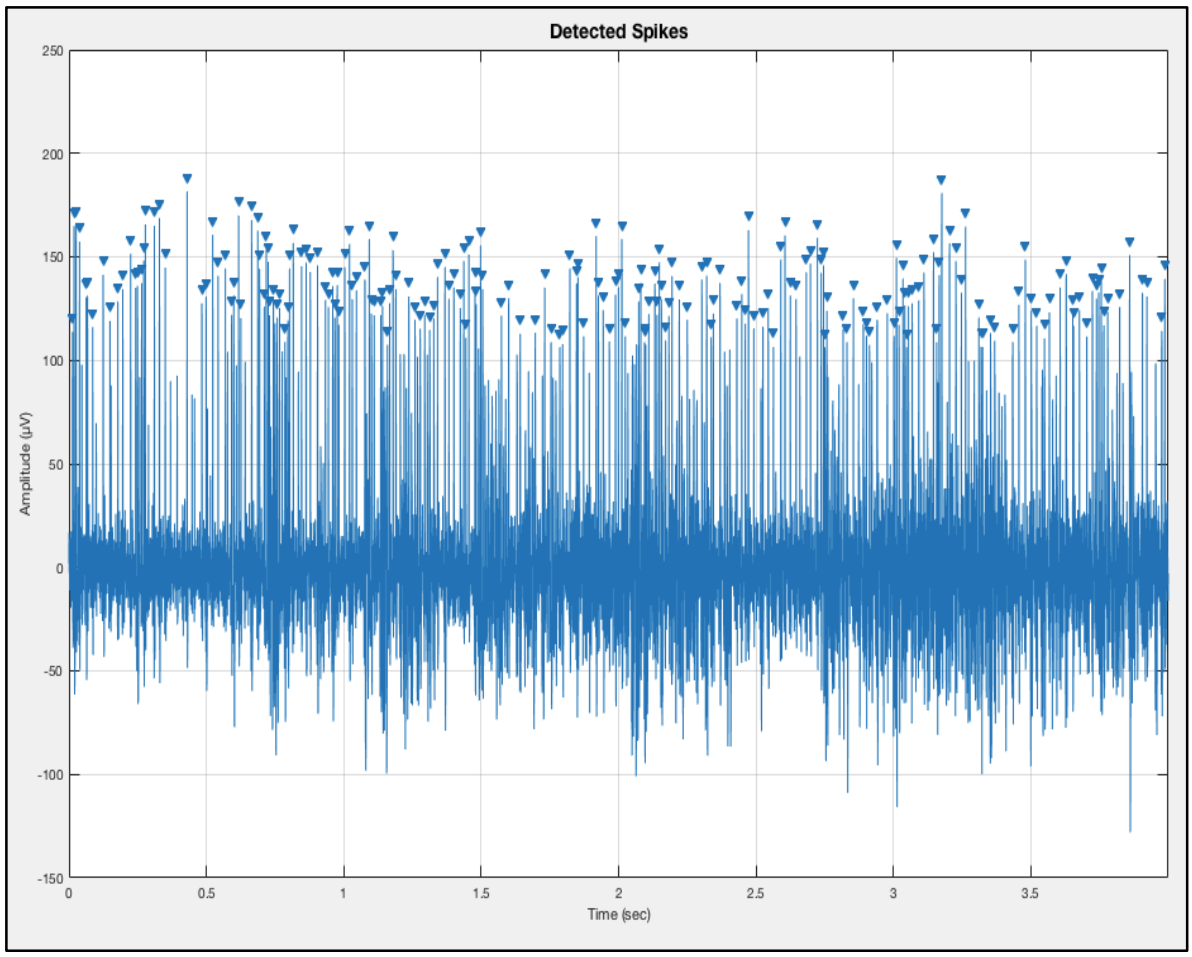

Figure:4.4: Spike detection (channel:1; trial:7).

Figure 4.5 illustrates a representative signal for spike sorting. After the detection of spikes, the detected spikes were clustered based on their amplitudes and spike widths using

the *kmeans* algorithm in MATLAB. In this example, the spikes were divided into four clusters.

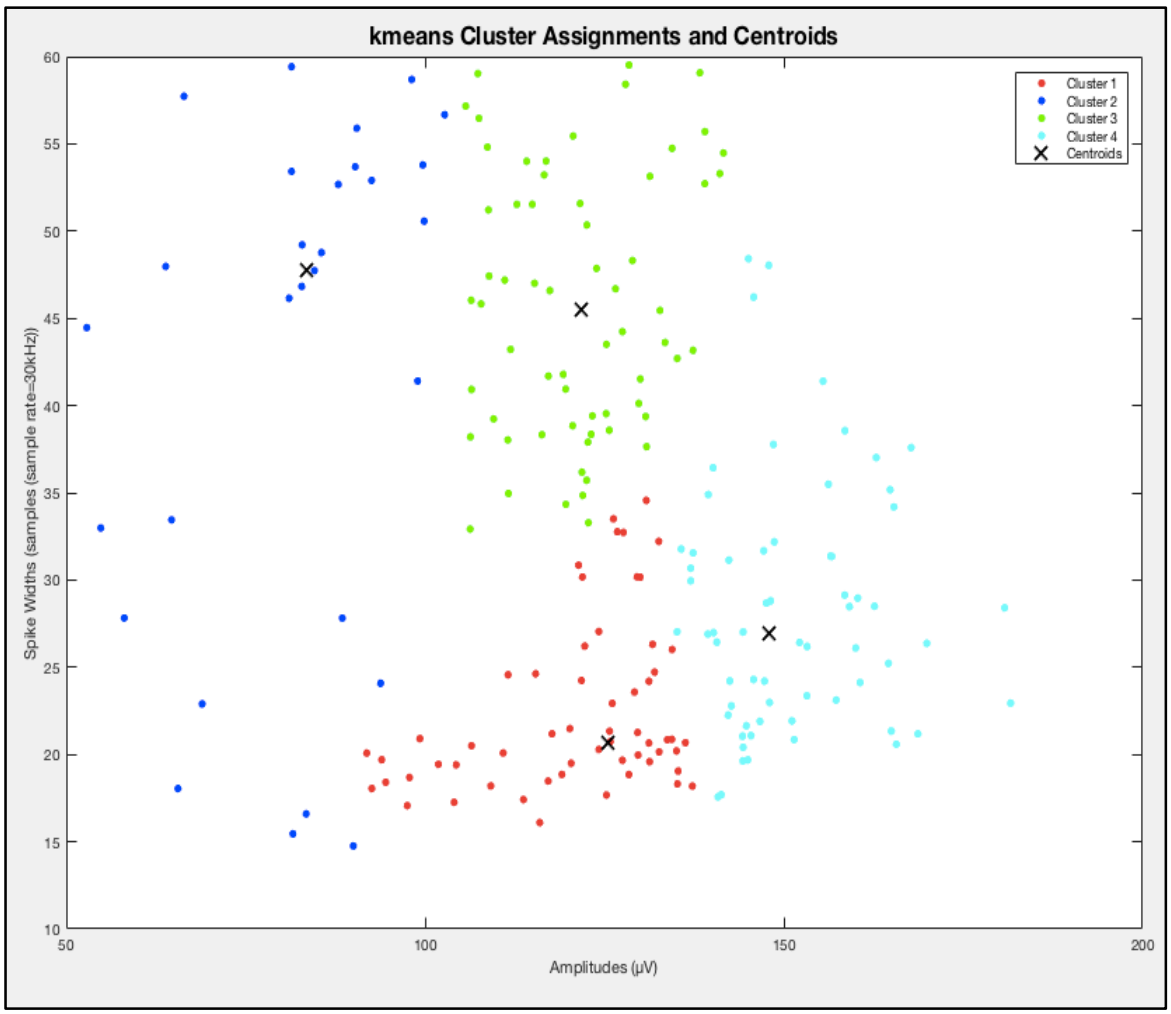

Figure 4.5: Clustering (channel:1; trial:7). The black 'x' indicate the cluster centers.

Figure 4.6 is the output of the spike sorting demonstrated in Figure 4.5. The spikes clustered in the previous example were plotted in separate windows by aligning them in time with respect to their peak point.

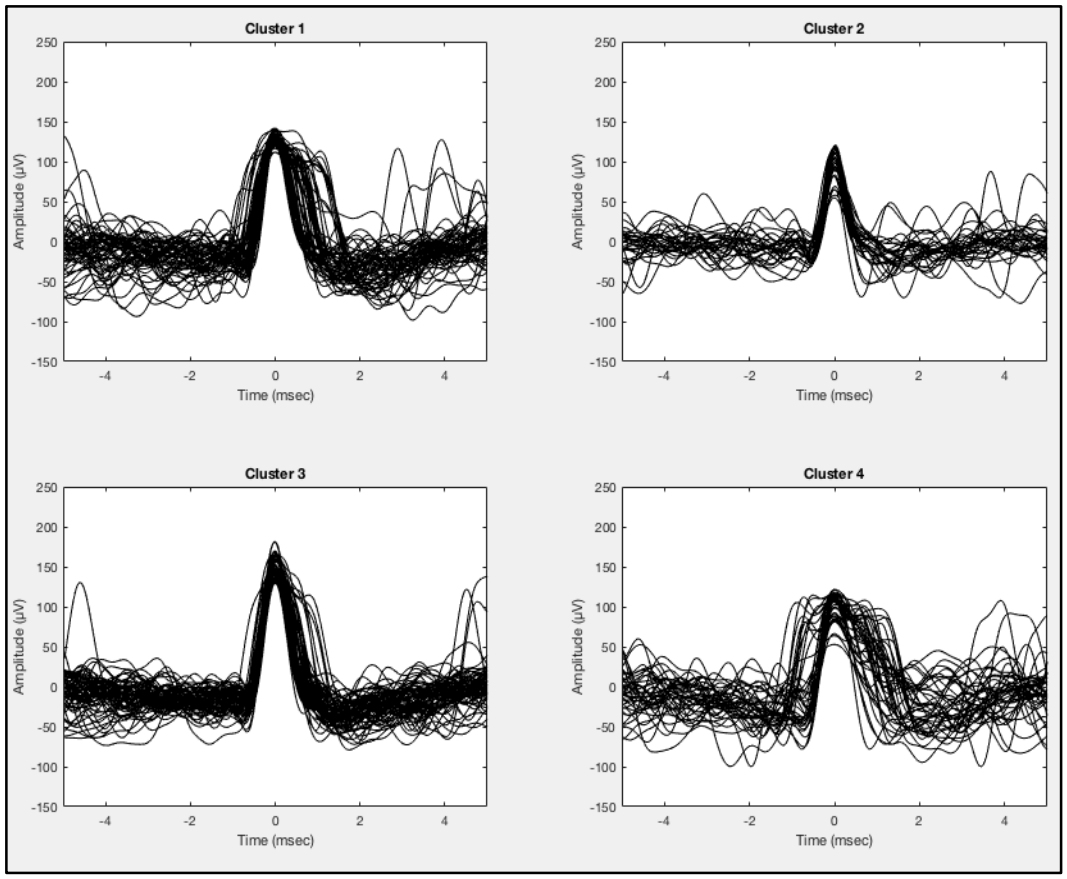

Figure 4.6: Spike sorting (channel:1; trial:7).

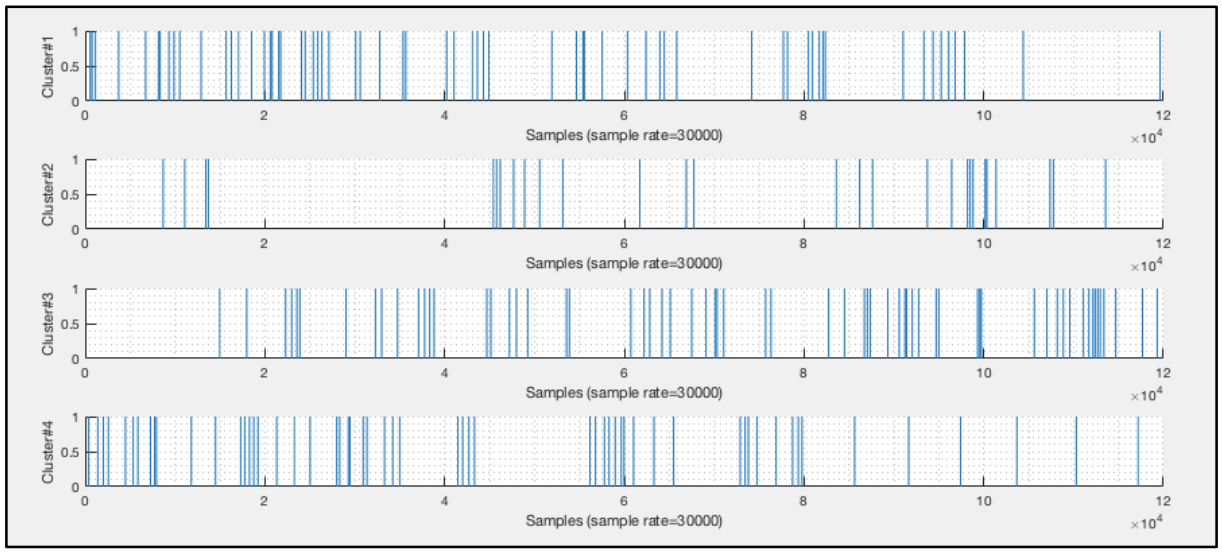

Figure 4.7: Sorted spikes` raster plots for each cluster (channel:1; trial:7).

Figure 4.8 and Figure 4.9 are other examples of the effect of different animal states on neural activity.

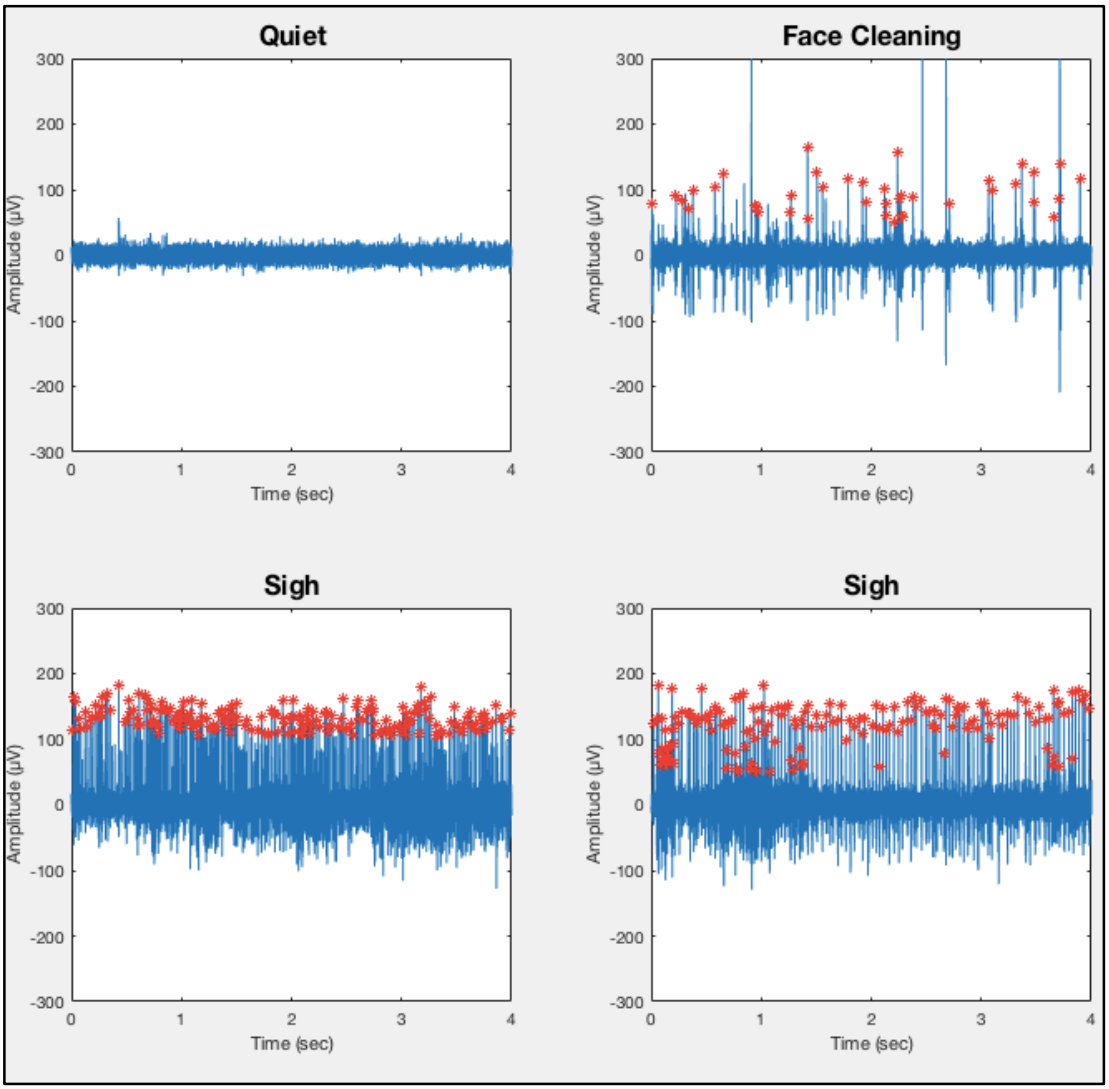

Figure 4.8: Spike activity change with animal state (channel:1; trials: 2, 18, 7, and 8).

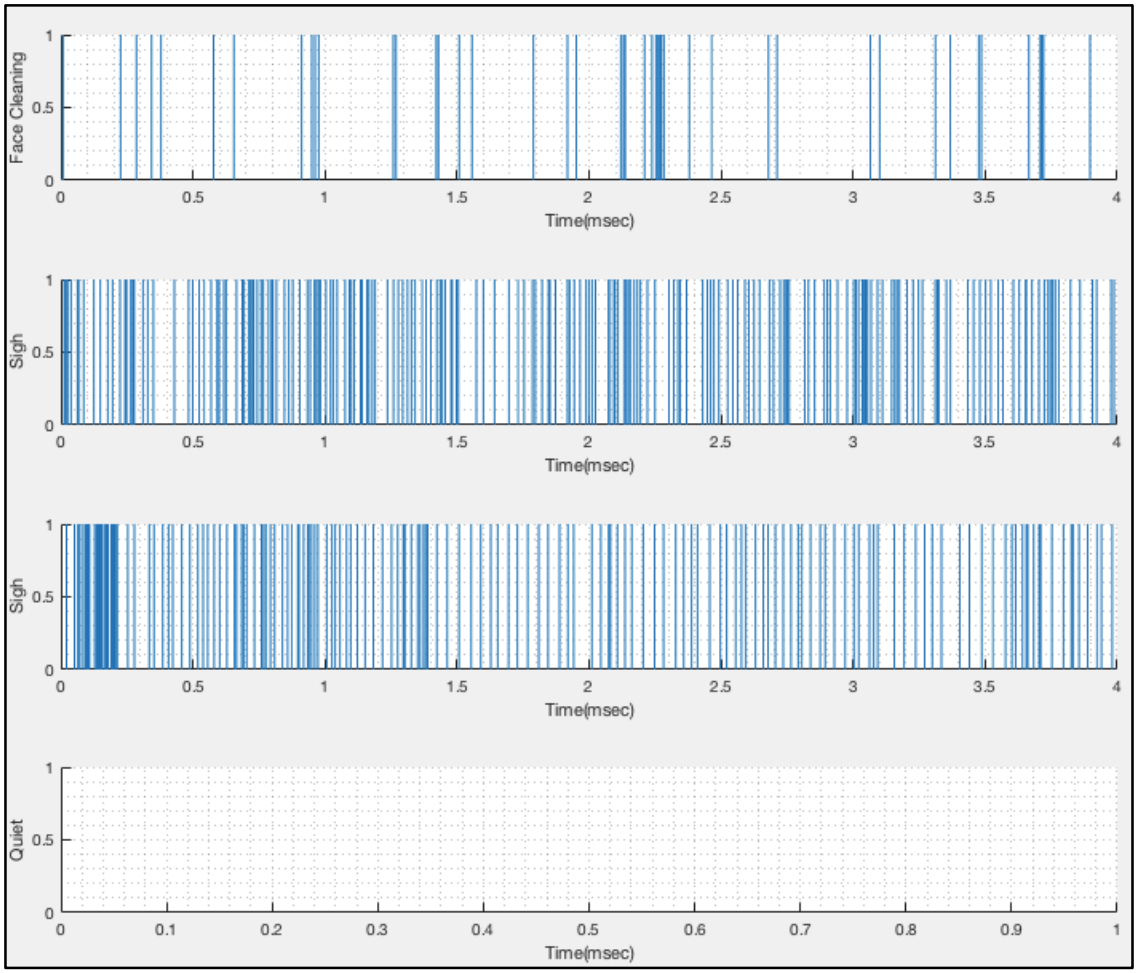

Figure 4.9: Raster plot (channel:1; trials: 2, 18, 7, and 8).

The firing rate in the same channel from different trials are shown in Figure 4.10. The number of spikes are counted in 50 ms long time bins. As seen in the figure, when the animal is active, firing rates increase significantly.

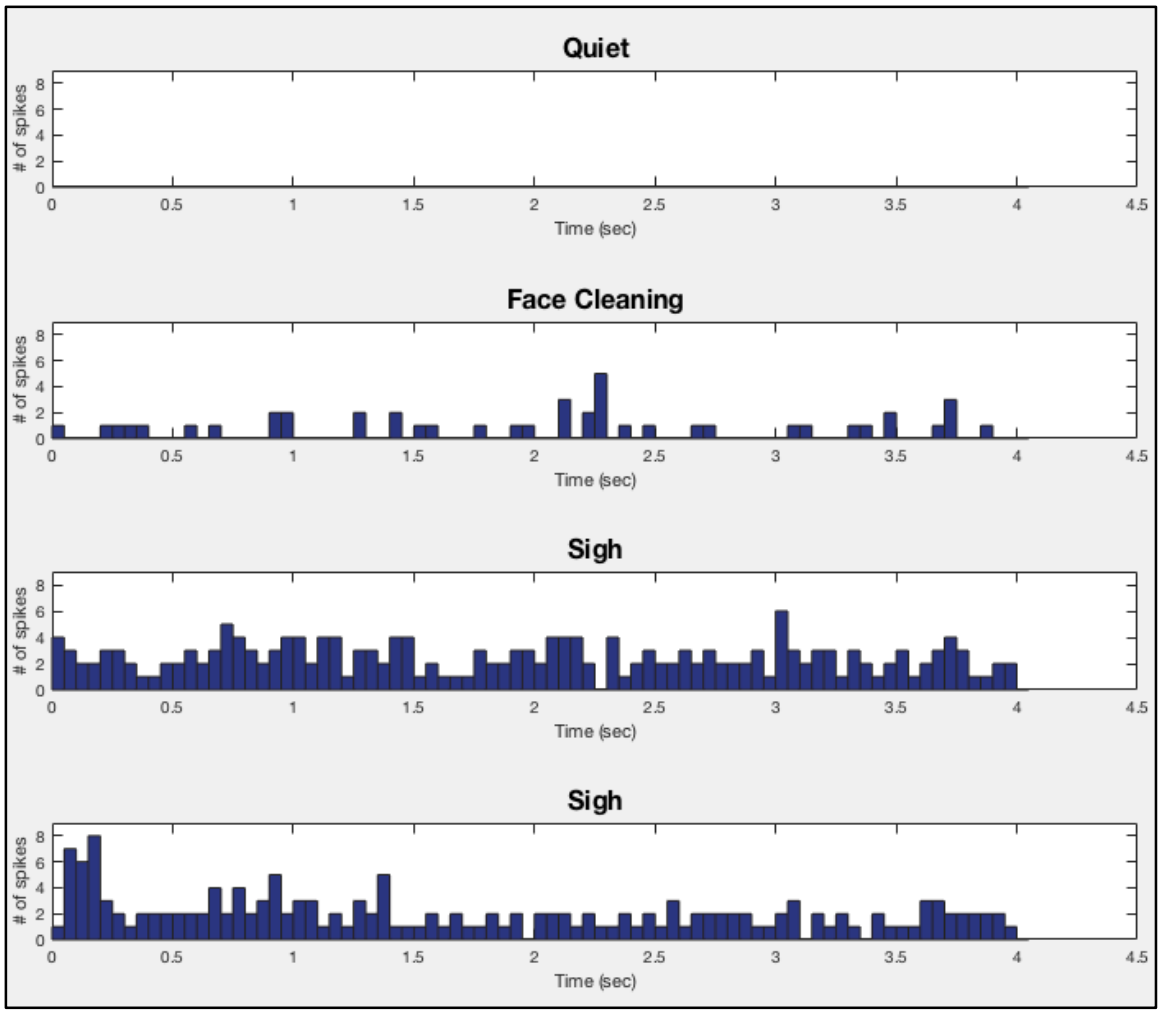

Figure 4.10: Firing rate (channel:1; trials: 2, 18, and 7).

The SNR values of the six trials from the selected channel were calculated as the ratio of the average of the peak-to-peak amplitude of the spikes to the standard deviation of the baseline noise. Figure 4.11 shows the evaluated signal sections and noise sections for this specific channel`s selected trials. Numbers in insets are SNR values.

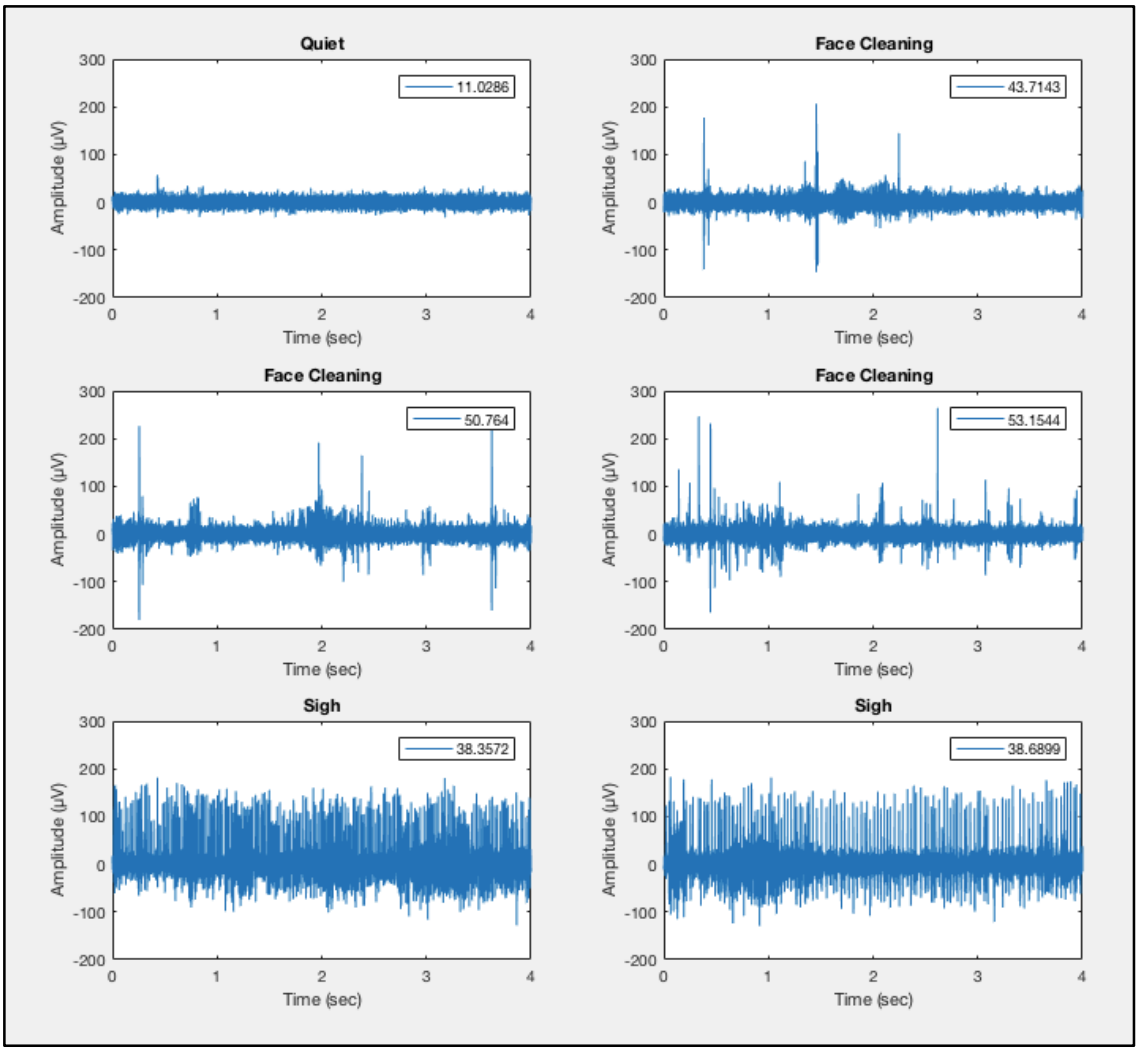

Figure 4.11: SNR values (channel:1; trials: 2, 34, 35, 38, 7, and 8).

The raster plot in Figure 4.12 is from two different channels and from all trials. This figure demonstrates that each channel records different signals in each trial when all trials of one session is evaluated. Additionally, this plot highlights that both channels record the same activity simultaneously in some time intervals marked by the circles.

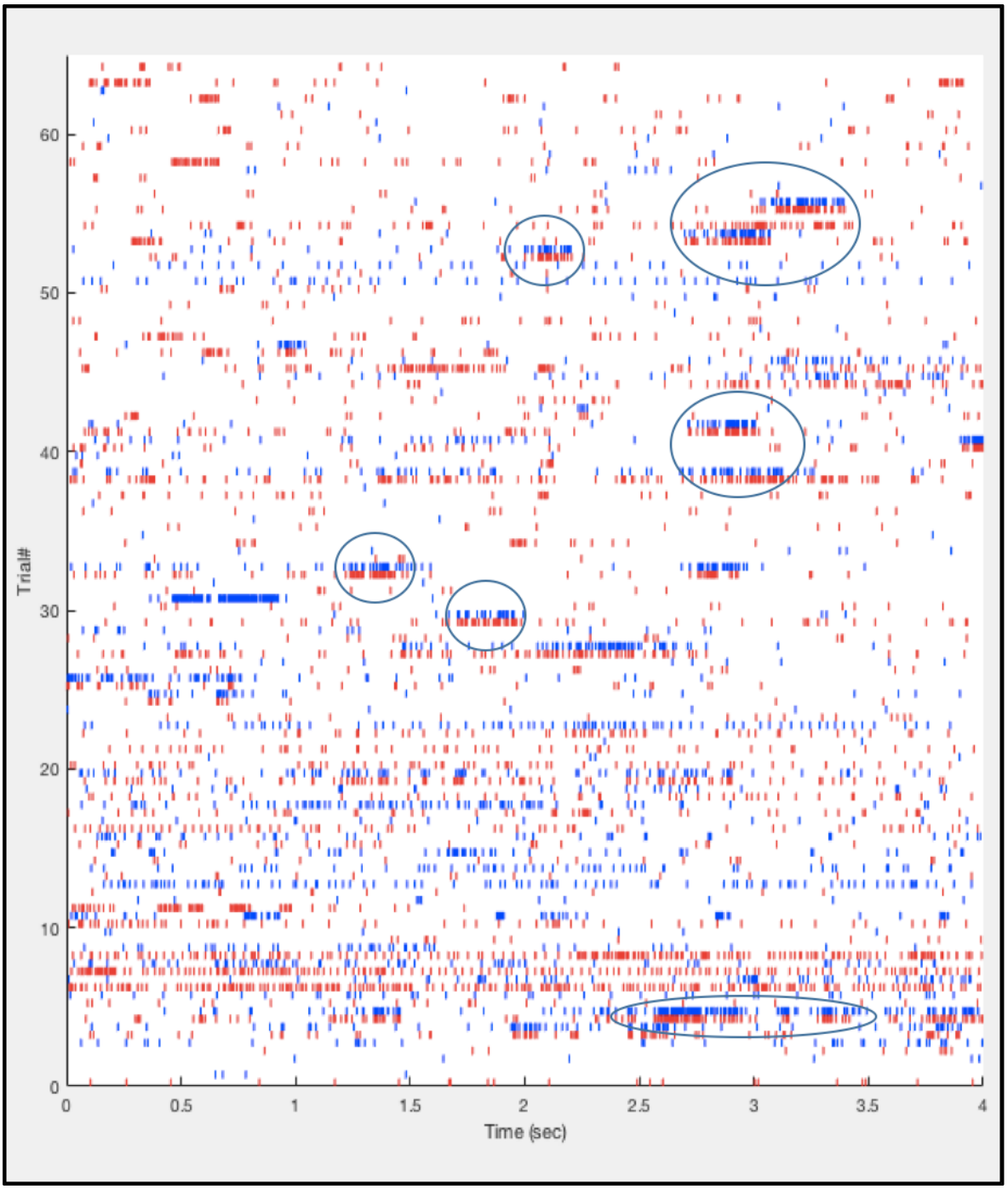

Figure 4.12: Raster plot (channel:1 and 32; all trials). Areas marked with circles indicate some of the time intervals when both channels record similar pattern of activity.

Session #3:

Figure 4.13 and the following raster plot (Figure 4.14) and firing rate (Figure 4.15) figures point out that channels were functional on this session as well. Additionally, the face cleaning activities had relatively similar patterns.

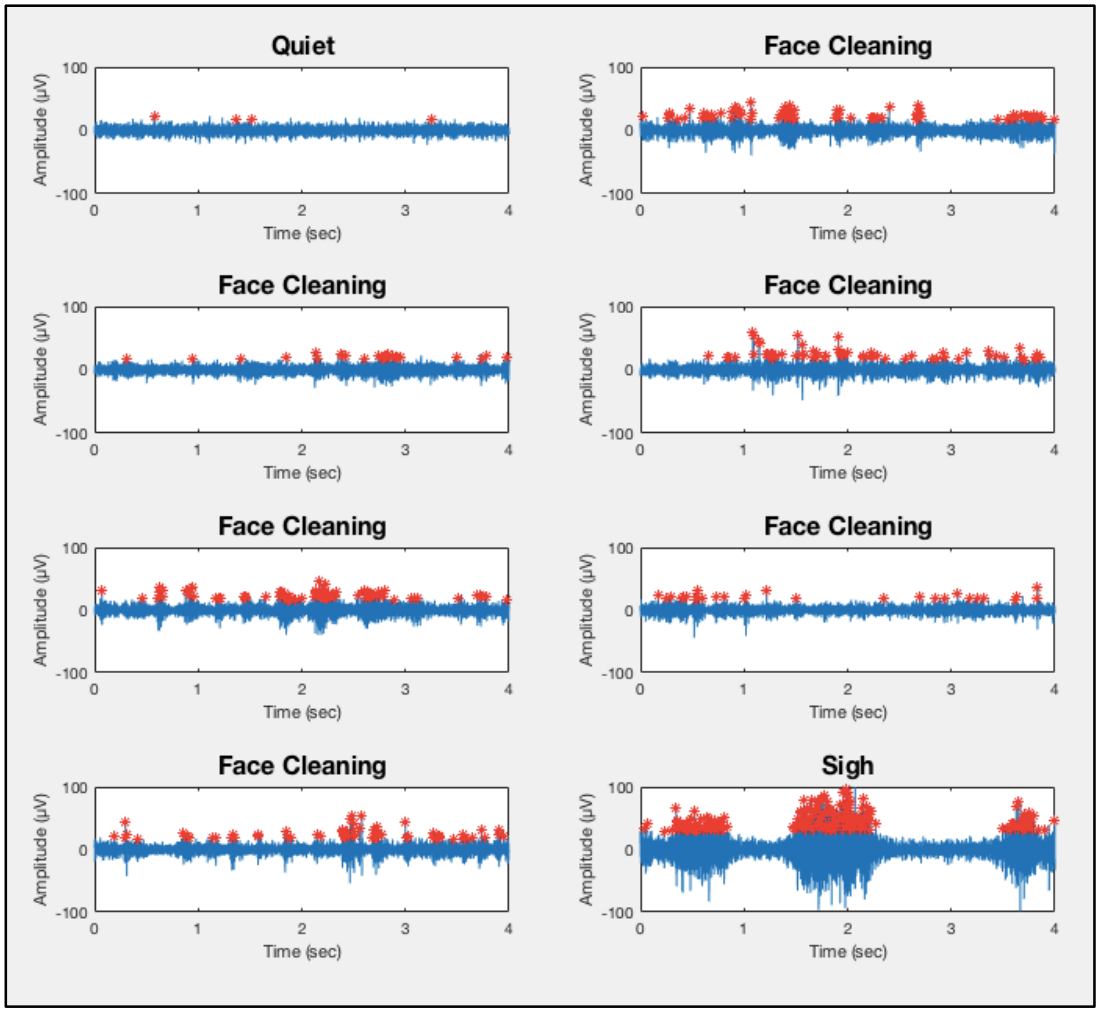

Figure 4.13: Spike activity change with animal state (channel:31; trials: 43, 30, 32, 33, 35, 36, 37, and 4).

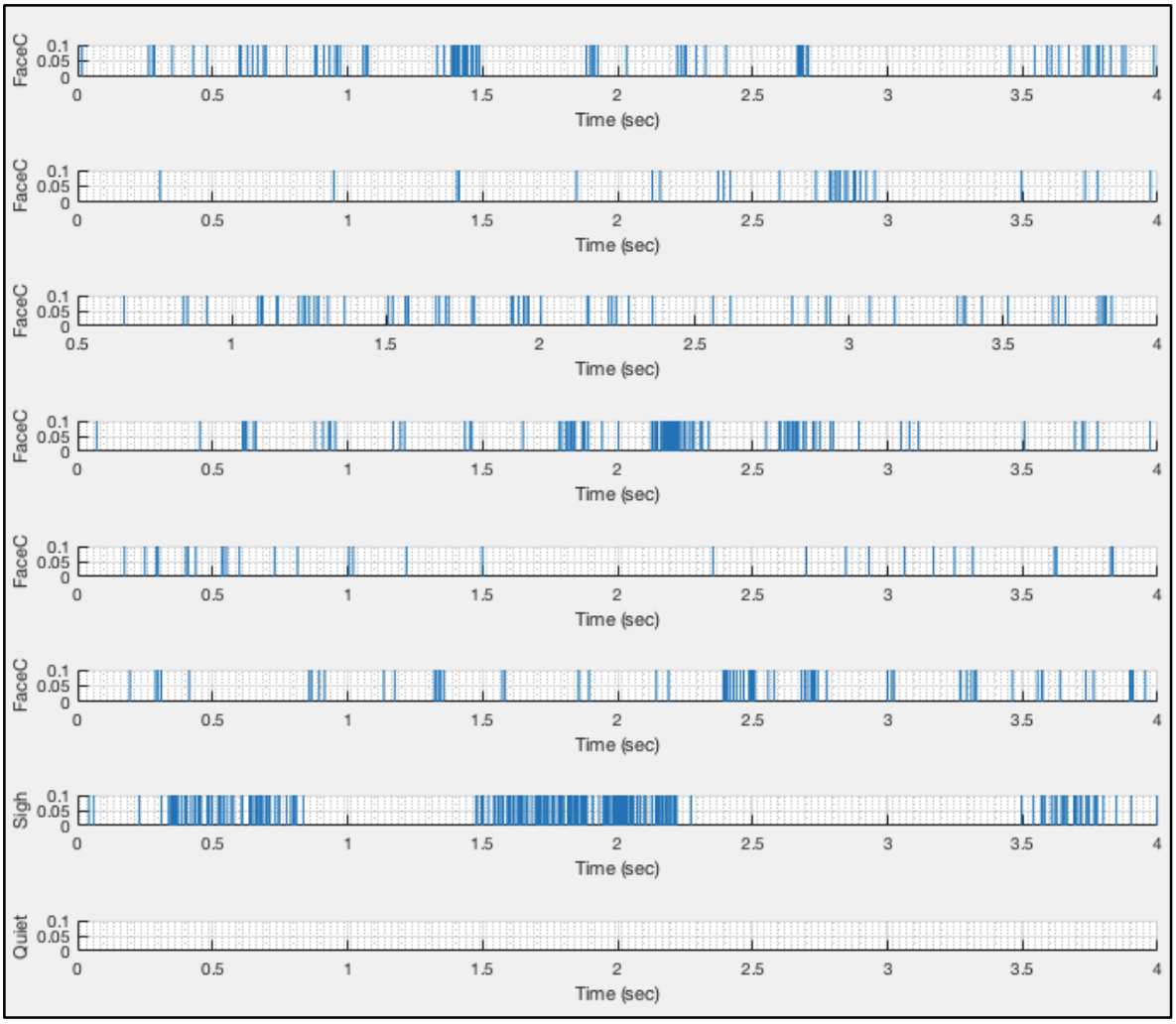

Figure 4.14: Raster plot (channel:31; trials: 43, 30, 32, 33, 35, 36, 37, and 4).

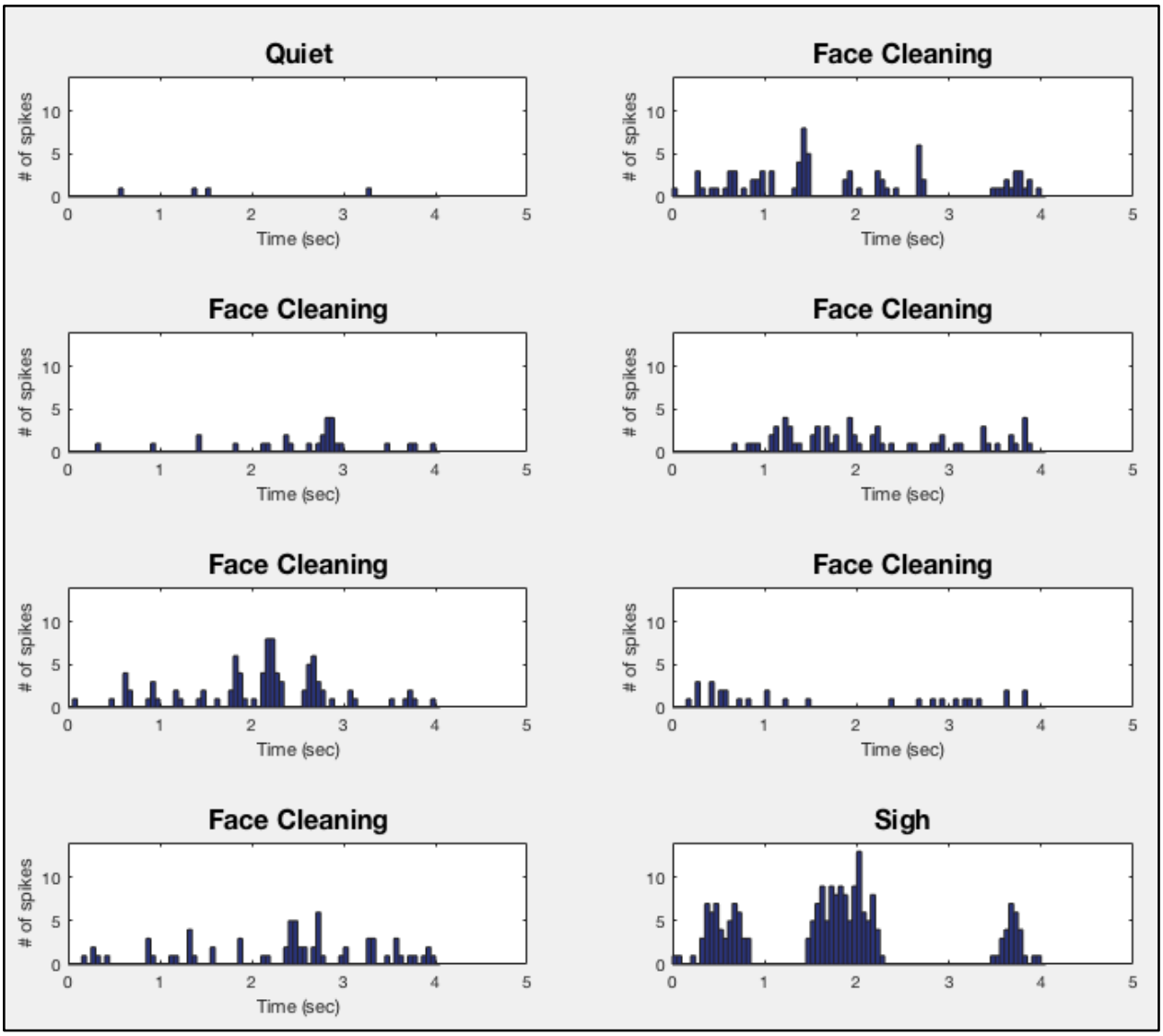

Figure 4.15: Firing rate (channel:31; trials: 43, 30, 32, 33, 35, 36, 37, and 4).

4.2.3 Immunohistochemistry

The histology images in Figure 4.16 are coronal sections from the implanted spinal cord from Rat#1. The immunohistochemistry results of the first animal showed that even though electrodes were bundled together, they still stayed apart as small groups in the tissue after implantation. Also, the limited encapsulation thickness around the electrode`s footprint is very mild.

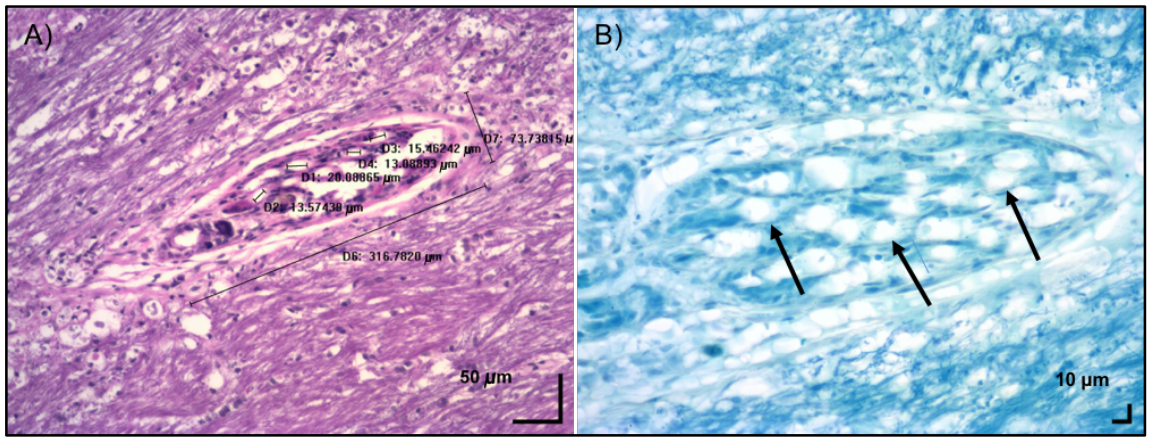

Figure 4.16: Immunohistochemistry coronal sections. A) H&E, B) LFB. Arrows indicate tissue response around the some of the carbon fibers.

4.3. The Results from Rat#2

4.3.1 *In vivo* Impedance Test:

In vivo impedance recordings were performed with Nipod (NeuroNexus Inc.) electrode tester. Impedance values of the desheathed channels were significantly lower than the control electrodes with single blunt cut. Additionally, it was observed that some of the desheathed channel impedances were small whereas others were similar to the control electrodes. The channels with low impedances were selected for evaluation.

The selected desheathed channels with low impedances are 7, 11, 13, 21, 25, 27, 29, and 31.

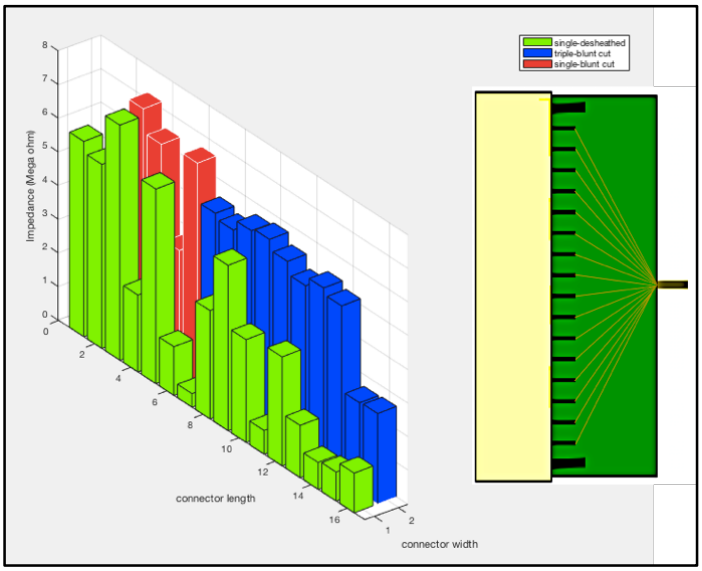

Figure 4.17: Impedance values of single blunt cut and triple blunt cut carbon fiber channels.

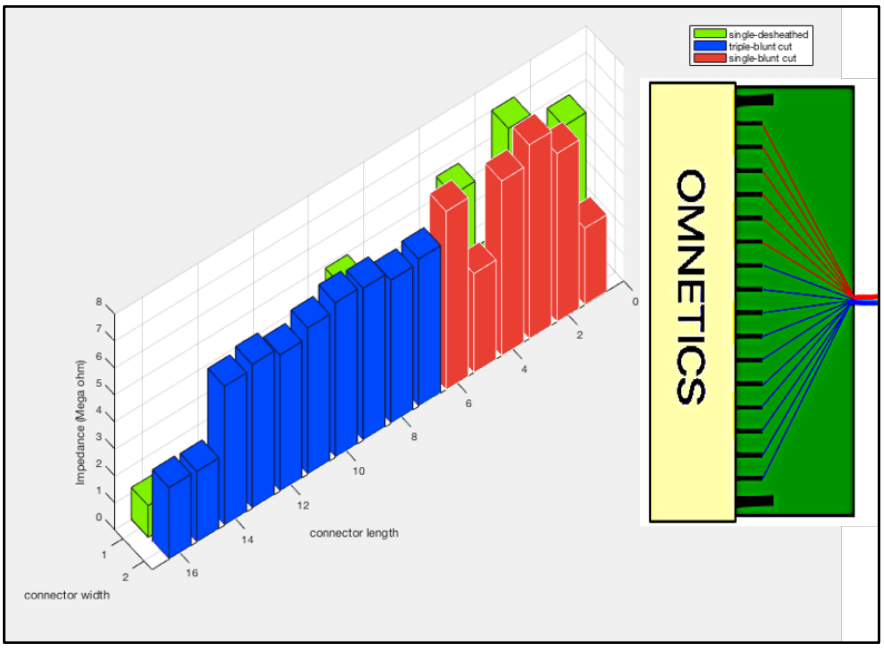

Figure 4.18: Impedance values of single desheathed carbon fiber channels.

Triple fiber electrode impedance values were also lower than that of the control electrodes but the difference was not very large.

All impedance values decreased over time. The following figure shows that impedances were extremely small after the 3rd session. Signals from the first three sessions were used for signal analysis since the drop of the impedance was interpreted as the electrode or its insulation being damaged.

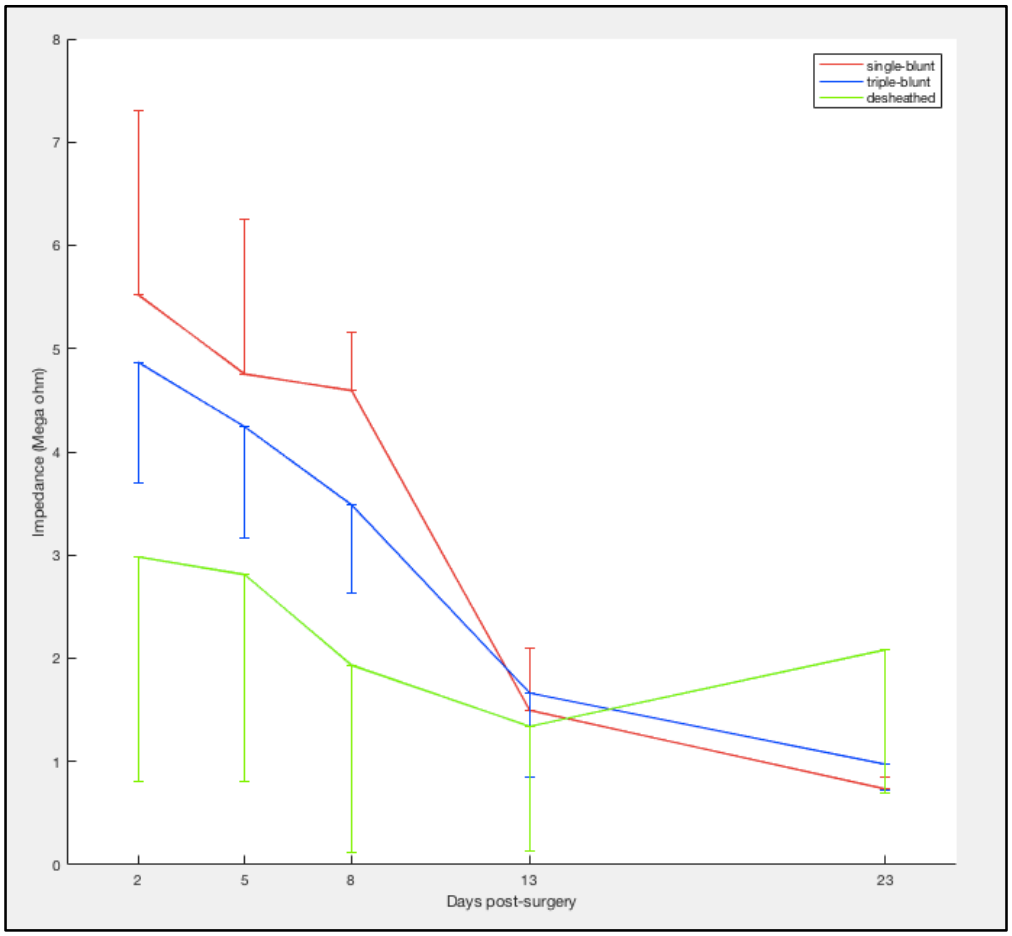

Figure 4.19: *In vivo* impedance values of all channels. The plot shows mean values and standard bars.

One way ANOVA test was performed and significant differences between control and desheathed group were found (Figure 4.20). The difference between control and triple channel groups was not significant according to the same test. Statistical evaluations were repeated for each session individually using a ANOVA test and similar results were found for Session#1 and #3, but no significant difference was detected among the three groups of Session#2.

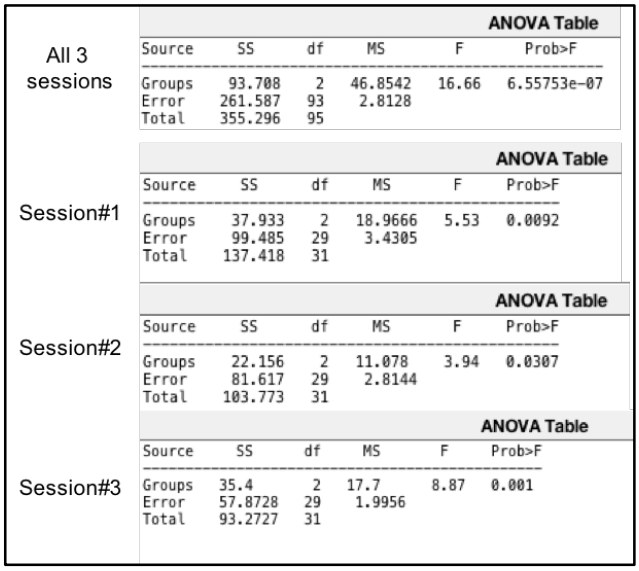

Figure 4.20: ANOVA test results (SS: sum of squares due to each source. df: degrees of freedom associated with each source. MS: Mean squares for each source. F: *F*-statistic. Prob>F: p-value).

4.3.2 Neural Signals:

Figure 4.21 summarizes the results of the second animal`s neural data. For each group spike counts and SNR values of simultaneously collected data were calculated.

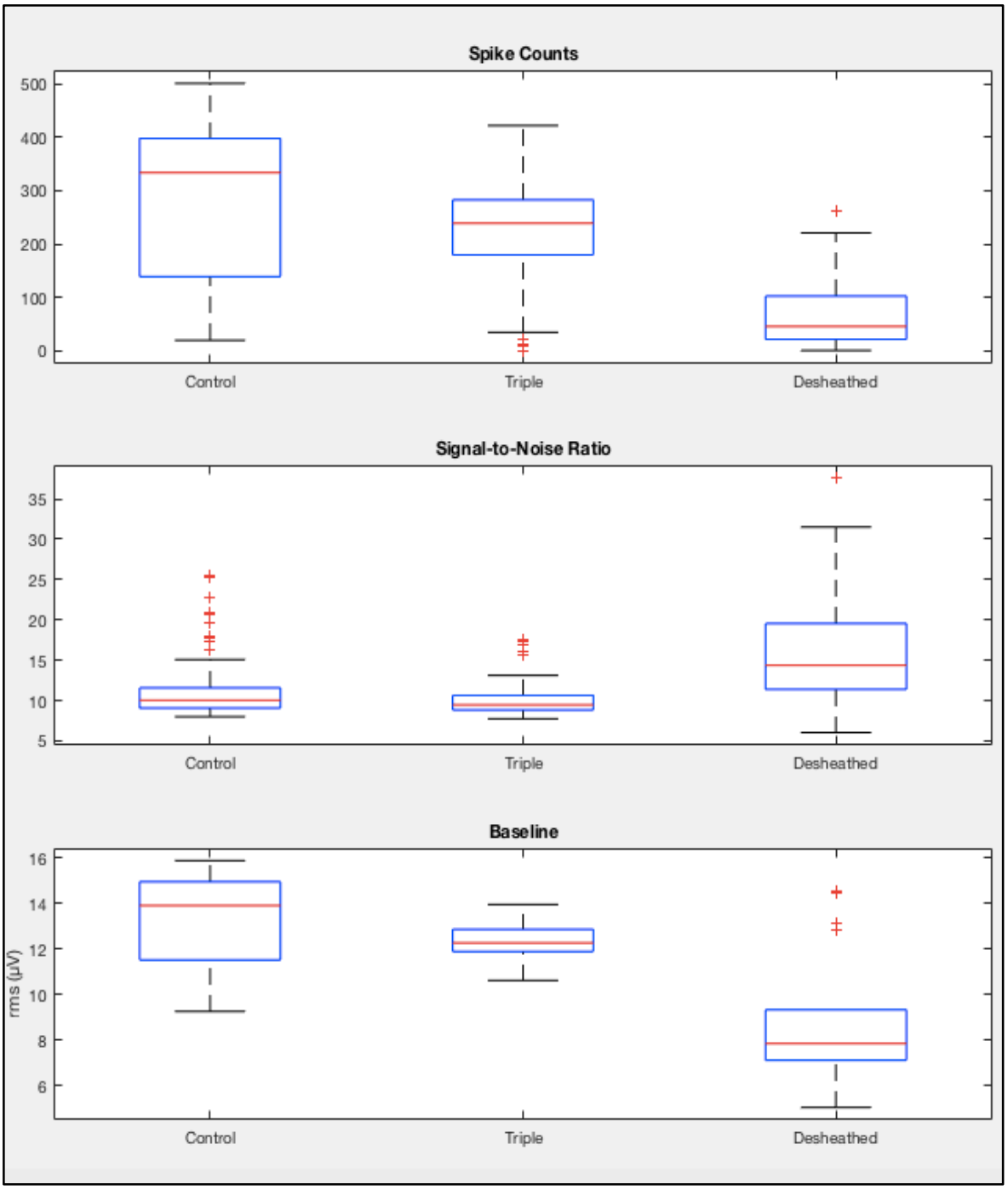

Figure 4.21: Spike counts, SNR values, and baseline noise values.

Table 4.2: Average Spike Counts, SNR Values, and Their Standard Deviations

	Mean	**± std**
Spike counts of control channels (n=6)	281	± 139
SNR values of control channels (n=6)	11.48	± 3.84
Spike counts of triple channels (n=10)	229	± 76
SNR values of triple channels (n=10)	10.11	± 2.09
Spike counts of desheathed channel (n=8)	68	± 62
SNR values of desheathed channels (n=8)	15.62	± 6.06

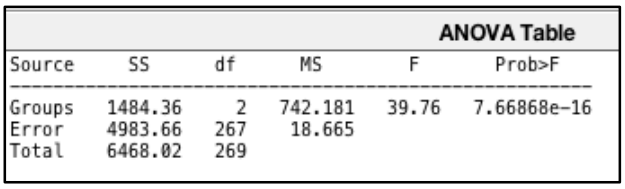

ANOVA Table

Source	SS	df	MS	F	Prob>F
Groups	1484.36	2	742.181	39.76	7.66868e-16
Error	4983.66	267	18.665		
Total	6468.02	269			

Figure 4.22: ANOVA result of the SNR values of different groups. Significance is achieved only between control and desheathed channel groups.

CHAPTER 5

CONCLUSION AND DISCUSSION

The results of the present study reaffirmed the suitability of carbon fiber electrodes for chronic neural activity recording. The electrode used in this work can be built in most research labs easily because of the simplicity of the procedure and the basic equipment required.

The SEM images indicate that parylene-C coating was thicker than the value expected as being 2.2 μm instead of 0.76 μm. However, the thicknesses of both plain carbon fiber and coated carbon fiber were varied along the length. The soldering iron desheathing technique was evaluated with SEM images. At the tip, the thickness was 6.4 μm, almost the same as the uncoated carbon fiber`s thickness. This confirms that desheathing was successful at the tip. The carbon fiber`s 200 μm length was desheathed, however the thickness was 7.4 μm where desheathing ended, which means some of the coating remained.

From the first animal`s state data (Figure 4.3) it can be seen at anesthetized episodes, the activity was at the baseline level. While waking up, the spikes started to be observed. In the active state, intense firings were detected. The comparison of recordings at different animal states, such as quiet and active, shows the correlation between spike activities and different animal behaviors. Figure 4.8, 4.9, and 4.10 show that similar animal behaviors result in similar signal patterns. The same conclusion can be reached from other sessions as well (Figure 4.11, 4.12, and 4.13)

During the current study, spikes were observed in the neural data. Spikes were detected in Figure 4.4 and 4.6 had amplitudes in the range of 100-200 μV and their durations were about 2 milliseconds, which is typical of neural action potentials.

The first animal`s spikes were sorted based on the spike width and amplitude. Since only spikes at the action potential frequency were selected with bandpass filtering, in general their widths were in the same range. Because of that, clustering was performed mainly based on the amplitude values. Different spike shapes might be a result of different distances between electrodes and recorded units. In Figure 4.6, particularly, spikes clustered into Cluster 1, 2, and 3 have distinctive spike shapes, which suggest that they are indeed from different neurons.

In Figure 4.12, each channel`s behavior during all trials demonstrates the variation of signals. Additionally, in the same figure in certain sections of the episodes (highlighted with circles on the figure) both channels recorded activities simultaneously. They may have recorded signals from the same unit or may be from different units that fired simultaneously.

Immunohistochemistry results in Figure 4.16 demonstrated that even though electrodes were in a bundle shape, they splayed in the tissue, which was prefered in terms of recording from different neurons or units simultaneously.

In vivo impedance measurements of the second animal matched our predictions. After desheathing it was expected to see significant impedance decrease because of the size of exposed surface area, and measurements confirmed that.

Among desheathed channels some of them had high impedances, which can be the result of the technique used. When carbon fiber filaments were desheathed, they were in a

bundle shape. The ones at the middle of the bundle probably did not make contact with the desheathing tube and because of that they may not have been desheathed properly. The desheathed channels with low impedances were selected and used in the data analysis.

There is also impedance decrease at the triple channels which is the result of tripled cross sectional area. Three times of cross sectional area ($3 \times \pi r^2 = 3 \times \pi * 3.5^2 = 115\ \mu m^2$) is very small compared to the sum of one cross sectional area multiplied by 75 μm length surface area of the cylinder ($\pi r^2 + 2\pi r * l = \pi * 3.5^2 + 2\pi 3.5 * 75 = 38.5 + 1649 = 1687.5\ \mu m^2$) as in the case of desheathing of 75 μm length. Because of this, a relatively larger impedance drop due to desheathing compared to triple filaments is plausible.

Impedances drastically dropped after the third session. This can be because of the peeling of coating material. However, we did not confirm that with SEM images of the explanted electrodes from rat #2.

Figure 4.21 suggests that desheathing decreases average spike counts, but increases SNR values. In the case of triple fiber electrodes, spike counts decreased as well, even though it was not as significant as desheathing. On the other hand, the SNR values of triple channels remained the same as the control group.

The spike counts of the desheathed channels were smallest compared to the other two groups. This can be the result of spatial averaging. Since the exposed recording area was bigger, the electrodes possibly recorded several units at the same time and it is possible that the signals from multiple cells canceled each other. The reason for high SNR values of desheathed channels is the low baseline noise, which is shown in the third plot of Figure 4.21.

FUTURE WORK

There is room for improvements in our electrode design. Spike counts drastically decreased with desheathed electrode channels. The desheated electrode length can be shortened to reduce the averaging effect to keep the spike counts high. To this end, more precise technique for desheathing can be developed, e.g. laser ablation, or the current system can be upgraded by using a smaller tube.

To be able to record from different neurons, channels should stay separated in tissue. This is difficult to achieve with a bundle electrode. The current electrode design can be improved by adopting a 2D array design using a template with precisely defined locations for the fiber tips. This template with a 2D arrangement of holes may be fabricated using deep reactive ion etching (DRIE) technique.

Impedance decrease over time can be a result of delamination of the coating. Covering electrodes with a thicker parylene-C layer can resolve this problem.

CHAPTER 6

APPENDIX

This appendix contains the MATLAB codes used in the analysis.

```
% Detect Spikes
i=1;        %Trial number
k=1;        %Channel number
fc1=100;                                % High-pass
fc2=1500;                               % Low-pass
h=50;                                   % MinPeakHeight
n=200;                                  % Maximum number of peaks
disp(['trial' num2str(Trials(i)) '.mat'])
trialname = ['trial' num2str(Trials(i)) '.mat'];
load(trialname)
fs = ripple_rate;
time = ripple_time';
data = ripple_data';
fn=[fc1*2/fs fc2*2/fs];                 % Frequency band. fs/2=Nyquist limit
[zn,pn,kn] = butter(4,fn,'bandpass');   % 4th order Butterworth filter
[sosn,gn] = zp2sos(zn,pn,kn);           % Zero-pole-gain to second-order sections model
conversion.
data_filt=filtfilt(sosn,gn,data);       % Filter x forwards and backwards, to avoid a time
delay
[pks,locs,widths,amps]=findpeaks(data_filt(:,k),fs,'MinPeakDistance',0.001,'SortStr',
'descend','MinPeakHeight',h,'Npeaks',n,'MinPeakProminence',100,'MaxPeakWidth',0.003);
plot(time, data_filt(:,k));
title('Spikes','FontSize', 16);
ylabel('Amplitude (uV)');
xlabel('Time (sec)');
hold on;
plot(locs,pks,'*r');
hold off;

% Raster Plot
t=locs;
for ii=1:length(t)                  % Loop through each spike time
    line([t(ii) t(ii)], [0 1])
end
    ylim([0 1]);
    xlabel('Time(msec)');
    ylabel('Trial#');
    grid MINOR;

% Firing Rate
N=zeros(81,1);                  % Initialize the Spike Count with zeros
                                % Loop over all trials
[N, BIN]=histc(locs,edges);     % Calculate how many spikes in the window(edge)
title('Firing Rate','FontSize',16)
xlabel ('Time (sec)')
ylabel ('# of spikes')
subplot(4,1,i)
bar(edges, N,'histc');              % Plot PETH as a bar graph

% SNR
k=2;i=2;                            %Baseline signal(quiet)
data_filtbaseline=filtfilt(sosn,gn,data(:,k)); % Filter x forwards and backwards, to avoid a
time delay
data_filtsignal=filtfilt(sosn,gn,data);       % Filter x forwards and backwards, to avoid a
time delay
SNR=peak2peak(data_filtsignal)/rms(data_filtbaseline);
plot(time,data_filtsignal)
legend(num2str(SNRT(i)));

% Feature Extraction
[pks,locs,widths,amps]=findpeaks(data_filt,'MinPeakDistance',0.005*fs,'MinPeakHeight',50,'MinPe
akProminence',100,'MaxPeakWidth',0.002*fs)
peaks=[];
peaks = [peaks; pks];
wdths=[];
wdths = [wdths; widths];
peaks = peaks';
```

```
wdths = wdths';
x=vertcat(peaks,wdths);
x=x';

% kmeans Clustering
opts = statset('Display','final');
c=4;        %Cluster number
no_of_vectors=2;
[idx,C,sumd,D] = kmeans(x,c,'Distance','cityblock','Replicates',10,'Options',opts);

figure
plot(x(idx==1,1),x(idx==1,2),'r.','MarkerSize',12)
hold on
plot(x(idx==2,1),x(idx==2,2),'b.','MarkerSize',12);
hold on
plot(x(idx==3,1),x(idx==3,2),'g.','MarkerSize',12);
hold on
plot(x(idx==4,1),x(idx==4,2),'c.','MarkerSize',12);

plot(C(:,1),C(:,2),'kx','MarkerSize',12,'LineWidth',2)
legend('Cluster 1','Cluster 2','Cluster 3','Cluster 4','Centroids','Location','NE')
xlabel('Amplitudes (?V)'); ylabel('Spike Widths (samples (sample rate=30kHz))')
title ('kmeans Cluster Assignments and Centroids','FontSize', 16)
hold off


%Spike Sorting
figure;

for j=1:numel(unique(idx))  % how many unique groups?
    ind = find(idx==j);     % find the index numbers of spikes that belong to a certain group
    ap = [];                % empty variable
    for k=1:numel(ind)
        st = locs(ind(k)) - fs*0.005 + 1;       % Start of the spike
        ed = locs(ind(k)) + fs*0.005;           % End of the spike
        ap(:,k) = data_filt(st:ed);             % Cropping the spike
    end
    subplot(2,2,j); plot(ap,'k'); title(num2str(j)); ylim([-150 250])
    xticks([30:60:290]);
    xticklabels({'-4' '-2' '0' '2' '4'})
end

% ANOVA
group = [repmat({'ControlD3'}, 6, 1); repmat({'TripleD3'}, 10, 1); repmat({'DesheathedD3'}, 16,
1)];
[p,tbl,stats] =
anova1([impedance_controlD3';impedance_tripleD3';impedance_desheathedD3'],group);
[c,~,~,gnames] = multcompare(stats);
[gnames(c(:,1)), gnames(c(:,2)), num2cell(c(:,3:6))];
```

REFERENCES

[1] K. D. W. Arnold C. Hoogerwerf, "A three-dimensional microelectrode array for chronic neural recording," *IEEE Trans Biomed Eng,* vol. 41, no. 12, pp. 1136 - 1146, December 1994.

[2] L. R. Hochberg *et al.*, "Neuronal ensemble control of prosthetic devices by a human with tetraplegia," *Nature,* vol. 442, no. 7099, pp. 164-71, Jul 13 2006.

[3] M. Alam, W. Rodrigues, B. N. Pham, and N. V. Thakor, "Brain-machine interface facilitated neurorehabilitation via spinal stimulation after spinal cord injury: Recent progress and future perspectives," *Brain Res,* vol. 1646, pp. 25-33, Sep 01 2016.

[4] N. A. Silva, N. Sousa, R. L. Reis, and A. J. Salgado, "From basics to clinical: a comprehensive review on spinal cord injury," *Prog Neurobiol,* vol. 114, pp. 25-57, Mar 2014.

[5] E. Z. D. o. B. S. a. E. B. E. Laboratory. (2017, 10/1/2017). *Electrophysiology & Neuroscience*. Available: https://www.bsse.ethz.ch/bel/research/electrophysiology-and-neuroscience.html

[6] M. E. Obien, K. Deligkaris, T. Bullmann, D. J. Bakkum, and U. Frey, "Revealing neuronal function through microelectrode array recordings," *Front Neurosci,* vol. 8, p. 423, 2014.

[7] M. Okun, A. Lak, M. Carandini, and K. D. Harris, "Long Term Recordings with Immobile Silicon Probes in the Mouse Cortex," *PLoS One,* vol. 11, no. 3, p. e0151180, 2016.

[8] H. Scherberger, M. R. Jarvis, and R. A. Andersen, "Cortical local field potential encodes movement intentions in the posterior parietal cortex," *Neuron,* vol. 46, no. 2, pp. 347-54, Apr 21 2005.

[9] M. M. Heinricher, "Neurophysiological techniques: applications to neural systems.," pp. 8-13.

[10] S. M. Wellman *et al.*, "A Materials Roadmap to Functional Neural Interface Design," *Advanced Functional Materials,* 2017.

[11] T. Takekawa, Y. Isomura, and T. Fukai, "Accurate spike sorting for multi-unit recordings," *Eur J Neurosci,* vol. 31, no. 2, pp. 263-72, Jan 2010.

[12] S. Y. Chang *et al.*, "Wireless fast-scan cyclic voltammetry to monitor adenosine in patients with essential tremor during deep brain stimulation," *Mayo Clin Proc,* vol. 87, no. 8, pp. 760-5, Aug 2012.

[13] R. C. Jean-Luc Ponchon, Francois Gonon, Michel Jouvet, and Jean-Francois Pujol, "Normal pulse polarograhy with carbon fiber electrodes for in vitro and in vivo determination of catecholamines," *Analytical Chemistry,* vol. 51, no. 9, pp. 1483 - 1486, August 1979.

[14] M. HajjHassan, V. Chodavarapu, and S. Musallam, "NeuroMEMS: Neural Probe Microtechnologies," *Sensors (Basel),* vol. 8, no. 10, pp. 6704-6726, Oct 25 2008.

[15] F. Vitale, S. R. Summerson, B. Aazhang, C. Kemere, and M. Pasquali, "Neural stimulation and recording with bidirectional, soft carbon nanotube fiber microelectrodes," *ACS Nano,* vol. 9, no. 4, pp. 4465-4474, 2015.

[16] R. G. Wilke, G. K. Moghadam, N. H. Lovell, G. J. Suaning, and S. Dokos, "Electric crosstalk impairs spatial resolution of multi-electrode arrays in retinal implants," *J Neural Eng,* vol. 8, no. 4, p. 046016, Aug 2011.

[17] G. Guitchounts, J. E. Markowitz, W. A. Liberti, and T. J. Gardner, "A carbon-fiber electrode array for long-term neural recording," *J Neural Eng,* vol. 10, no. 4, p. 046016, Aug 2013.

[18] P. R. Patel *et al.*, "Chronic in vivo stability assessment of carbon fiber microelectrode arrays," *J Neural Eng,* vol. 13, no. 6, p. 066002, Dec 2016.

[19] A. G. Purves D, Fitzpatrick D, et al., *Neuroscience*, 2nd Edition ed. (Neural Circuit). Sunderland (MA): Sinauer Associates, 2001.

[20] C. A. Tobias *et al.*, "Delayed grafting of BDNF and NT-3 producing fibroblasts into the injured spinal cord stimulates sprouting, partially rescues axotomized red nucleus neurons from loss and atrophy, and provides limited regeneration," *Experimental Neurology,* vol. 184, no. 1, pp. 97-113, 2003.

[21] M. A. Nicolelis and M. A. Lebedev, "Principles of neural ensemble physiology underlying the operation of brain-machine interfaces," *Nat Rev Neurosci,* vol. 10, no. 7, pp. 530-40, Jul 2009.

[22] J. D. Simeral, S. P. Kim, M. J. Black, J. P. Donoghue, and L. R. Hochberg, "Neural control of cursor trajectory and click by a human with tetraplegia 1000 days after implant of an intracortical microelectrode array," *J Neural Eng,* vol. 8, no. 2, p. 025027, Apr 2011.

[23] R. A. Ramadan, S. Refat, M. A. Elshahed, and R. A. Ali, "Basics of Brain Computer Interface," in *Brain-Computer Interfaces*(Intelligent Systems Reference Library, 2015, pp. 31-50.

[24] J. J. Shih, D. J. Krusienski, and J. R. Wolpaw, "Brain-computer interfaces in medicine," *Mayo Clin Proc,* vol. 87, no. 3, pp. 268-79, Mar 2012.

[25] Jonathan R. Wolpaw, Niels Birbaumer, Dennis J. McFarland, Gert Pfurtscheller, and T. M. Vaughan, "Brain–computer interfaces for communication and control," *Clinical Neurophysiology,* vol. 113, pp. 767-791, 2002.

[26] (10/15/2017). *File:Cfaser haarrp.jpg (1 October 2005 (original upload date) ed.)*. Available: https://commons.wikimedia.org/wiki/File:Cfaser_haarrp.jpg

[27] (10/15/2017). *What is carbon fiber?* Available: http://www.carbonfiber.gr.jp/english/material/what.html

[28] (10/15/2017). *Carbon Fiber used in Fiber Reinforced Plastic (FRP)*. Available: http://www.build-on-prince.com/carbon-fiber.html

[29] P. R. Patel, "Carbon fiber microelectrode array for neuroprosthetic and neuroscience applications," Doctorate, Biomedical Engineering, The University of Michigan, Michigan.

[30] Z. T. Group. (2017, 9/22/2017). *What is carbon fiber?* Available: http://zoltek.com/carbonfiber/

[31] S. R. Vala Vivek, "Government engineering college - bhavnagar (021)," ed: Slide share, 2016.

[32] R. Fairless *et al.*, "Preclinical retinal neurodegeneration in a model of multiple sclerosis," *J Neurosci,* vol. 32, no. 16, pp. 5585-97, Apr 18 2012.

[33] C. Y. Johannes W. Rohen, Elke Lutjen-Drecoll, *Color atlas of anatomy*, 7th Edition ed. Wolters Kluwer, Lippincott Williams & Wilkins.

[34] F. E. B. Larry R. Squire, Nicholas C. Spitzer, Sascha du Lac, Anirvan Ghosh, Darwin Berg, *Fundamental Neuroscience*, 3rd Edition ed. Elsevier, 2008.

[35] P. M. Roos, "Studies on metals in motor neuron disease," Institute of environmental medicine, Karolinska Institutet, Stockholm, 2013.

[36] C. F. Vogelaar and V. Estrada, "Experimental Spinal Cord Injury Models in Rodents: Anatomical Correlations and Assessment of Motor Recovery," in *Recovery of Motor Function Following Spinal Cord Injury*, 2016.

[37] J. M. Armstrong-James Michael, "Carbon fibre microelectrodes," *Journal of Neuroscience Methods,* vol. 1, pp. 279-287, 1979.

[38] D. Budai, "Carbon fiber-based microelectrodes and microbiosensors," in *Intelligent and Biosensors*, vol. January 2010, V. S. Somerset, Ed., 2010.

[39] A. Piironen, M. Weckstrom, and M. Vahasoyrinki, "Ultrasmall and customizable multichannel electrodes for extracellular recordings," *J Neurophysiol,* vol. 105, no. 3, pp. 1416-21, Mar 2011.

[40] N. B. L. Takashi D. Yoshida Kozai, Paras R. Patel, Xiaopei Deng, Huanan Zhang, Karen L. Smith, Joerg Lahann, Nicholas A. Kotov & Daryl R. Kipke, "Ultrasmall implantable composite microelectrodes with bioactive surfaces for chronic neural interfaces," *Nature Materials* vol. 11, pp. 1065-1073, 2012.

[41] P. R. Patel *et al.*, "Insertion of linear 8.4 mum diameter 16 channel carbon fiber electrode arrays for single unit recordings," *J Neural Eng,* vol. 12, no. 4, p. 046009, Aug 2015.

[42] M. S. Abhishek Prased, "Extraction of motor activity from the cervical spinal cord of behaving rats," *J Neural Eng,* vol. 3, no. 4, pp. 287-292, 2006.